Cancer Immunology, Immunotherapy (2023) 72:4123–4144
https://doi.org/10.1007/s00262-023-03547-8

RESEARCH

Apolipoprotein C-III itself stimulates the Syk/cPLA2-induced inflammasome activation of macrophage to boost anti-tumor activity of $CD8^+$ T cell

Xiangyu Hu[1] · Shizhen Ding[1] · Guotao Lu[2] · Zhijie Lin[1] · Liting Liao[1] · Weiming Xiao[2] · Yanbing Ding[2] · Yu Zhang[3,6] · Zhengbing Wang[4] · Weijuan Gong[1,2,5,6] · Xiaoqin Jia[1]

Received: 23 March 2023 / Accepted: 11 September 2023 / Published online: 18 October 2023

Abstract

Increased prevalence of cancer in obese individuals is involved with dyslipidemia- induced chronic inflammation and immune suppression. Although apolipoprotein C-III (ApoC3)-transgenic mice ($ApoC3^{TG}$ mice) or poloxamer 407 (P407)-treated mice had hyperlipidemia, $CD8^+$ T cells with upregulated antitumor activities were observed in $ApoC3^{TG}$ mice, and decreased $CD8^+$ T cell activities were observed in P407-treated mice. Increased ApoC3 expression in hepatocellular carcinoma was associated with increased infiltration of $CD8^+$ T cells and predicted survival. Recombinant ApoC3 had no direct effects on $CD8^+$ T cells. The upregulation of $CD8^+$ T cells in $ApoC3^{TG}$ mice was due to cross-talk with context cells, as indicated by metabolic changes and RNA sequencing results. In contrast to dendritic cells, the macrophages of $ApoC3^{TG}$ mice ($macrophages^{TG}$) displayed an activated phenotype and increased IL-1β, TNF-α, and IL-6 production. Coculture with $macrophages^{TG}$ increased $CD8^+$ T cell function, and the adoptive transfer of $macrophages^{TG}$ suppressed tumor progression in vivo. Furthermore, spleen tyrosine kinase (Syk) activation induced by TLR2/TLR4 cross-linking after ApoC3 ligation promoted cellular phospholipase A2 (cPLA2) activation, which in turn activated NADPH oxidase 2 (NOX2) to promote an alternative mode of inflammasome activation. Meanwhile, mitochondrial ROS produced by increased oxidative phosphorylation of free fatty acids facilitated the classical inflammasome activation, which exerted an auxiliary effect on inflammasome activation of $macrophages^{TG}$. Collectively, the increased antitumor activity of $CD8^+$ T cells was mediated by the ApoC3-stimulated inflammasome activation of macrophages, and the mimetic ApoC3 peptides that can bind TLR2/4 could be a future strategy to target liver cancer.

Keywords ApoC3 · $CD8^+$ T · Antitumor · Inflammasome · Macrophage

Abbreviations

ApoC3	Apolipoprotein C-III
Syk	Spleen tyrosine kinase
cPLA2	Cellular phospholipase A2
sPLA2	Secreted PLA2
P407	Poloxamer 407
HCC	Hepatocellular carcinoma
IL-1β	Interleukin-1β
TNF-α	Tumor necrosis factor α

Co-first authors: Xiangyu Hu and Shizhen Ding.

✉ Xiaoqin Jia
xqjia@yzu.edu.cn

[1] Department of Basic Medicine, School of Medicine, Yangzhou University, Yangzhou 225001, People's Republic of China

[2] Department of Gastroenterology, The Affiliated Hospital of Yangzhou University, Yangzhou University, Yangzhou 225001, People's Republic of China

[3] School of Nursing, Yangzhou University, Yangzhou 225001, People's Republic of China

[4] Department of General Surgery, The Affiliated Hospital of Yangzhou University, Yangzhou University, Yangzhou 225001, People's Republic of China

[5] Jiangsu Key Laboratory of Integrated Traditional Chinese and Western Medicine for Prevention and Treatment of Senile Diseases, Yangzhou 225001, People's Republic of China

[6] Jiangsu Key Laboratory of Zoonosis, Yangzhou 225001, People's Republic of China

IL-6	Interleukin-6
TLR2	Toll-like receptor 2
TLR4	Toll-like receptor 4
NADPH	Nicotinamide adenine dinucleotide phosphate
ROS	Reactive oxygen species
cROS	Cytoplasmic ROS
mROS	Mitochondrial ROS
MetSs	Metabolic syndromes
VLDL	Very-low-density lipoprotein
HDL	High-density lipoprotein
HTG	Hypertriglyceridemia
DCs	Dendritic cells
$ApoC3^{TG}$	ApoC3-transgenic
$CD36^{-/-}$	CD36 knockout
IHC	Immunohistochemical
AJCC	American joint committee on cancer
ATCC	American tissue culture collection
CPT1α	Carnitine palmitoyltransferase 1α
SREBP1/2	Sterol regulatory element binding protein 1/2
CGI58	Comparative gene identification-58
ATGL	Adipose triglyceride lipase
PD-L1	Programmed death-ligand 1
NKG2D	Natural killer group 2D
KLRG1	Killer-cell lectin like receptor G1
IFN-γ	Interferon-γ
IL-10	Interleukin-10
TGF-β	Transforming growth factor-β
GlUT1	Glucose receptor
HK II	Hexokinase II
ACC1	Acetyl-CoA carboxylase 1
p-ACC1	Phospho-ACC1
mTOR	Mammalian target of rapamycin
mTORC1	MTOR complex 1
LKB1	Liver kinase B1
AMPK	AMP kinase
Akt	Protein kinase B
PPARγ	Peroxisome proliferators-activated receptor γ
FOXO1	Forkhead box protein O1
NLRP3	NOD-like receptor family pyrin domain containing 3
Cas1	Caspase 1, cysteinyl aspartate specific proteinase 1
Cas8	Cysteinyl aspartate specific proteinase 8
c-Cas1	Cleaved caspase 1
c-Cac8	Cleaved caspase 8
RIPK1	Receptor-interacting protein kinase 1
GSDMD	Gasdermin D
PI3K p110α	Phosphatidylinositol 3-kinase p110α
NF-κB	Nuclear transcription factor-κB
NOX2	NADPH oxidase
CCDC109A	Coiled-coil domain containing 109A
FITC	Fluorescein isothiocyanate
PI	Propidium iodide
CFSE	5,6-Carboxyfluorescein diacetate, succinimidyl ester
DCFH-DA	2,7-Dichlorodihydrofluorescein diacetate
PVDF	Polyvinylidene fluoride
ECAR	Extracellular acidification rate
OCR	Oxygen consumption rate
LPS	Lipopolysaccharide
LDH	Lactate dehydrogenase
ANOVA	Analysis of variance
FFAs	Free fatty acids
TCGA	The cancer genome atlas
TME	Tumor microenvironment
OVA	Ovalbumin
WT	Wild type
PA	Palmitic acid
NAC	*N*-acetyl-*L*-cysteine
TRPM2	Transient receptor potential cation channel
FA	Flufenamic acid
FAO	Fatty acid oxidation
DEGs	Differentially expressed genes
KEGG	KYOTO encyclopedia of genes and genomes
HY	Hybrid mice, $ApoC3^{TG}$-$CD36^{\pm}$ mice

Introduction

Obesity is not only involved in metabolic syndromes (MetSs) related to various diseases, such as dyslipidemia, hypertension, type 2 diabetes, cardiovascular diseases, and nonalcoholic fatty liver disease, but also increases cancer incidence in at least 13 anatomical sites in adults [1, 2]. In overweight individuals, increased production of adipokines have been observed (e.g., adiponectin, chemerin, and leptin), which recruit immune cells, including macrophages and T cells, into adipose tissues [3, 4]. Persistent inflammation generates reactive oxygen species (ROS) and other toxic molecules, thus inducing the malignant transformation of normal cells [5]. Moreover, chronic obesity promotes the induction M2 macrophages, myeloid-derived suppressive cells, and regulatory T cells and mediates immune evasion in vivo [6, 7]. However, there are some studies show that elevated body mass index is associated with increased survival [8, 9]. Hence, the accurate and detailed subtyping of cancer patients with obesity should be incorporated into clinical diagnosis, therapy, and prognosis.

Apolipoprotein C-III (ApoC3) is an apoprotein synthesized by the liver and small intestine and has a molecular mass of 9 kDa. In circulation, ApoC3 is mainly associated with very-low-density lipoprotein (VLDL) and chylomicron,

and to a lesser extent, with high-density lipoprotein (HDL) [10]. ApoC3 modulates the metabolism of triglyceride-rich lipoproteins by inhibiting lipoprotein lipase and the hydrolysis of triglycerides and is involved in hepatic VLDL assembly and secretion [11, 12]. Hypertriglyceridemia (HTG) is an obvious characteristic of ApoC3-transgenic mice ($ApoC3^{TG}$ mice) [13]. Elevated ApoC3 levels in the plasma has been associated with atherosclerosis [14], type 2 diabetes [15], pancreatitis [16], and nonalcoholic fatty liver diseases [17]. The ApoC3 promoter polymorphisms C-482T and T-455C, in association with plasma triglycerides, are detected in individuals with metabolic syndromes [18, 19]. In hepatocellular carcinoma (HCC), high ApoC3 expression indicates increased survival [20, 21]. However, whether ApoC3 in HCC affects the tumor immune microenvironment should be clarified.

NK cell activities were decreased by lipid-induced metabolic reprogramming and cross-talk with local lipid-laden dendritic cells (DCs) in $ApoC3^{TG}$ mice [22]. When we subcutaneously injected tumor cells into $ApoC3^{TG}$ mice, tumor growth in vivo was unexpectedly suppressed. In the present study, we showed that the antitumor activities of $CD8^+$ T cells in $ApoC3^{TG}$ mice were upregulated by macrophage activation. The molecular mechanisms of macrophage functions affected by ApoC3 itself and hyperlipidemia were then investigated.

Materials and methods

Animals

$ApoC3^{TG}$ mice with ICR background were generated by crossing C57BL/6-$ApoC3^{TG}$ mice from Jackson Laboratory (Maine, USA) with wild-type (WT) ICR mice. Poloxamer 407 (P407; 0.5 g/kg; Sigma-Aldrich) was used to induce HTG in mice with a previously described method [22]. CD36 knockout ($CD36^{-/-}$) mice with C57BL/6 background were obtained from Jackson Laboratory (Maine, USA). A hybrid mouse line ($ApoC3^{TG}$–$CD36^{+/-}$ mice) was generated by crossing $CD36^{-/-}$ mice with $ApoC3^{TG}$ mice. All 8-week-old male WT mice with ICR or C57BL/6 background were purchased from Comparative Medical Center of Yangzhou University (Yangzhou, China). All animal experiments were approved by the institutional animal care and use committee of Yangzhou University (Yangzhou, China).

Patients and biopsies

The biopsies of 49 patients with HCC, including cancerous and paracancerous tissues, were collected for immunohistochemical (IHC) analysis. Pathological results were read by two experienced pathologists independently. The characteristics of patients with HCC are provided in Table S1. The stages of the patients were determined according to the guidelines provided in AJCC Cancer Staging Manual Eighth Edition (2017). This study was approved by the ethics committee of the Affiliated Hospital of Yangzhou University and obtained informed consent from all the patients.

Cells and reagents

H22, MC38, and B16F10 cells (mouse hepatoma, colon carcinoma, and melanoma cell lines respectively) were obtained from ATCC (VA, USA). Mouse $CD8^+$ T cells, macrophages, and DCs were isolated from the spleens and sorted out using magnetic beads (Miltenyi, Germany). The reagents used were as follows: recombinant mouse ApoC3 protein (ab226264), anti-ApoC3 (ab108205), anti-CPT1α (ab234111), anti-sterol regulatory element binding protein (SREBP) 1 (ab28481), anti-SREBP2 (ab30682), anti-CGI58 (ab183739), and anti-ATGL (ab207799), which were purchased from Abcam (Cambridge, UK). Rapamycin, compound C, LY294002, wortmanin, *N*-acetyl-*L*-cysteine, MCC950, Z-IETD-FMK, Z-YVAD-FMK, CAY10605, Varespladid, R406, flufenamic acid, etomoxir, and mito-TEMPO were purchased from MedChemExpress (NJ, USA). Antibodies for mouse CD3 (17A2), CD8 (53–6.7), CD44 (IM7), NKG2D (CX5), KLRG1 (2F1/KLRG1), CD62L (MEL-14), CD69 (H1.2F3), CD11b (M1/70), CD11c (N418), F4/80 (BM8), CD86 (GL-1), CD206 (C068C2), CD40 (3/23), PD-L1 (10F.9G2), CD36 (HM36), TLR2 (QA16A01), TLR4 (SA15-21), IFN-γ (XMG1.2), IL1β (NJTEN3), IL6 (MP5-20F3), IL-10 (JES5-16E3), TNF-α (MP6-XT22), TGF-β (TW7-16B4), and CD107a (1D4B) were obtained from BioLegend (CA, USA). Anti-mouse β-actin (13E5), GlUT1 (D3J3A), HKII (C64G5), acetyl-CoA carboxylase 1 (ACC1; C83B10), p-ACC (D7D11), mammalian target of rapamycin (mTOR; 7C10), p-mTOR (D9C2), mTORC1 (24C12), S6 (5G10), p-S6 (D57.2.2E), liver kinase B1 (LKB1; D60C5), AMP kinase (AMPK; D5A2), p-AMPK (D4D6D), Akt (C67E7), p-Akt (D9E), PPAR-γ (81B8), forkhead box protein O1 (FOXO1; C29H4), NLRP3 (D4D8T), caspase 8 (D35G2), cleaved caspase 8 (c-Cas8; D5B2), caspase 1 (Cas-1; E2Z1C), cleaved caspase 1 (c-Cas1; E2G2I), GSDMD (L60), cleaved-GSDMD (E3E3P), IL-1β (D3H1Z), cleaved-IL-1β (E7V2A), TLR2 (E1J2W), TLR4 (D8L5W), PI3K p110α (C73F8), NF-κB p65 (D14E12), NF-κB p-p65 (93H1), p38 (D13E1), p-p38 (D3F9), Erk (137F5), p-Erk (D13.14.4E), JNK (9252), and p-JNK (81E11) antibodies were obtained from Cell Signaling Technology (MA, USA). Anti-phospholipase A2 (PLA2) G4F (C-6), spleen tyrosine kinase (Syk; 4D10), and CCDC109A (E-9) antibodies were purchased from Santa Cruz Biotechnology (Texas, USA). Anti-cPLA2 (PLA2 G4A, YT1084) and anti-p-Syk

(YP0615) antibodies were obtained from ImmunoWay (Texas, USA). Anti-RIPK1 (38/RIP) antibody was obtained from BD Biosciences (NJ, USA), and anti- NADPH oxidase 2 (NOX2; 19013-1-AP) antibody was obtained from Proteintech (Illinois, USA). The antibody dosage used in the experiment was based on the manufacturer's instructions.

Flow cytometry

Mononuclear cells isolated from the spleens or other tissues were isolated and stained with corresponding fluorescent antibodies at 4 °C for 30 min and detected directly by flow cytometry. For intracellular cytokine analysis, the cells were treated with a fixation/permeabilization solution kit (BD Biosciences, NJ, USA) according to the manufacturer's instructions. For the analysis of cell degranulation, $CD8^+$ T cells were mixed with target cells (MC38 cells) in round-bottomed 96-well plates. After 2 h, 2 μM monensin (BD Biosciences) was added to the wells for another 2 h. The cells were stained with anti-mouse CD107a antibodies and analyzed by flow cytometry. For apoptosis assay, cells were detected with FITC Annexin V apoptosis detection kit (BD Biosciences) according to the manufacturers' instructions. For cell proliferation, the cells were labeled with 5 μM CFSE (Invitrogen, CA, USA). Mito-Tracker green indicator (Beyotime, Shanghai, China), DCFH-DA (Beyotime, Shanghai, China), and MitoSOX Indicator (Thermo Fisher Scientific, MA, USA) were used in evaluating the mitochondria, cytoplasmic ROS (cROS), and mitochondrial ROS (mROS) of cells respectively. Experimental methods and assay referred to the instructions of each kit. All data were analyzed with Flowjo V10 software.

Tumor models in mice

Tumor cells (2×10^6/ml) at the logarithmic growth phase were collected and subcutaneously injected into the back of each mouse. In mice with $CD8^+$ T cell depletion, anti-mouse CD8α depletion antibody was intraperitoneally injected at a dosage of 10 mg/kg every 3 days from one week before the injection of tumor cells to the day when mice were sacrificed. In the adoptive transfer of macrophages, $F4/80^+$cells (5×10^5) from $ApoC3^{TG}$ or WT mice were injected into tail veins of tumor-bearing mice every 2 days. Tumor size was recorded every 2 days. After 3 or 4 weeks, the mice were sacrificed for further analysis.

Western blot

Proteins from lysed cells were separated using sodium dodecyl sulfate–polyacrylamide gel electrophoresis, transferred to polyvinylidene fluoride (PVDF) membrane, and incubated with primary antibodies. After the PVDF membranes were incubated with horseradish peroxidase-conjugated secondary antibodies, the proteins were detected through chemiluminescence and quantified by ImageJ software.

In vivo depletion of macrophages

The mice were intraperitoneally injected with clodronate liposomes (LIPOSOMES, Netherlands) at a dosage of 10 ml/kg every 48 h for 1 week. The control liposome containing only PBS was used in parallel.

Immunohistochemistry

IHC staining was performed according to standard procedures. The staining results were analyzed according to optical density with Image Pro Plus software, and the percentage of positive cells was determined through semi-quantification [23]. Two pathologists assessed the grades separately. For immunofluorescence, cells were fixed on glass slides, permeabilized, blocked, and incubated with specific primary antibodies at 4 °C overnight. Immediately after staining with fluorescent secondary antibodies, the cells were observed under a confocal microscope.

Oxygen consumption rate (OCR) and extracellular acidification rate (ECAR)

The extracellular acidification rates (ECARs) and oxygen consumption rates (OCRs) of the cells were measured with XF96 extracellular flux analyzers (Seahorse Bioscience, MA, USA). $CD8^+$ T cells or macrophages (2×10^5) were aliquoted into the cells in Seahorse plates precoated with CellTak. The cells were cultured in a Seahorse medium containing 10 mM glucose, 2 mM glutamine, and 1 mM pyruvic acid. After centrifugation at 200*g* for 1 min, the plate was transferred to a CO_2-free incubator at 37 °C for 25 min for the complete adhesion of cells. The cells were treated with glucose (10 mM), oligomycin (1 μM), and 2-DG (100 mM), and glycolytic activities in the cells were evaluated. Mitochondrial respiratory activity was assessed with a XF cell Mito Stress Test kit (Seahorse Bioscience, MA,

USA). Glycolytic and oxidative phosphorylation capacities were calculated as previously described [22].

RNA-Seq

$CD8^+$ T cells and macrophages (5×10^6) were isolated and sorted out from the spleens of some mice. Each sample was treated with Trizol (Life Technologies, CA, USA) for the extraction of total RNAs. The degradation and contamination of RNAs were checked using agarose gels. In the absence of degradation and contamination, RNAs were subjected to subsequent experiments and analyzed as previously described [22].

IL-1β detected by ELISA

Macrophages (5×10^5) were treated with lipopolysaccharide (LPS, 200 ng/ml) for 12 h and Nigericin (10 μM) for 1 h. IL-1β released by macrophages in the supernatants were determined with a mouse IL-1β ELISA kit (Fcmacs, Nanjing, China) according to the manufacturer's instructions.

Measurement of lactate dehydrogenase (LDH)

Macrophages were stimulated with LPS (200 ng/ml) for 12 h and Nigericin (10 μM) for 1 h in an RPMI 1640 medium without phenol red. The cell supernatants of the macrophages were collected, and lactate dehydrogenase (LDH) level was determined according to the instructions of the LDH assay kit (Beyotime, Shanghai, China).

Detection of intracellular droplets and free fatty acids (FFAs)

Cells were stained with Nile red (Sigma-Aldrich, Darmstadt, Germany) for intracellular lipid droplet assessment. Lipid droplets were directly observed through confocal microscopy or quantified by flow cytometry. Intracellular free fatty acids (FFAs) were extracted using an assay for FFA solutions (Solarbio, Shanghai, China) and measured by colorimetry (550 nM) according to the instructions of the colorimetry kit's manufacturer.

Statistical analysis

Data were presented as mean ± standard deviation. Differences between two groups were evaluated using Student's t-test, and analysis of variance (ANOVA) was used in comparing more than two groups. Spearman's correlation coefficient for ranked data was used in determining the correlation of ApoC3 level in HCC with infiltrated $CD8^+$ T cells. All analysis was performed with GraphPad Prism 9. Significances of differences were indicated as follows: *, $P < 0.05$; **, $P < 0.01$; and ***, $P < 0.001$.

Results

Elevated number and bioactivity of $CD8^+$ T cells in $ApoC3^{TG}$ mice

Although the levels of triglycerides, cholesterol, and FFAs obviously increased in the plasma of $ApoC3^{TG}$ mice [22], the frequencies and number of $CD8^+$ T cells in the spleen or peripheral blood of the $ApoC3^{TG}$ mice unexpectedly increased (Fig. 1A). The $ApoC3^{TG}$ mice had more activated ($NKG2D^+$ or $CD44^+$) and effector ($CD44^+$ $KLRG1^+$ or $CD62L^-$ $CD44^+$) $CD8^+$ T cells (Fig. 1B and Supplementary Fig. S1A). The $CD8^+$ T cells of $ApoC3^{TG}$ mice had higher IFN-γ levels and increased degranulation (CD107a on membrane) when cocultured with MC38 cells (Fig. 1C). Meanwhile, apoptosis was inhibited in $CD8^+$ T lymphocytes derived from $ApoC3^{TG}$ mice (Fig. 1D and Supplementary Fig. S1B), whereas cell division was promoted (Fig. 1E). Collectively, the number of $CD8^+$ T cells and their activities increased in $ApoC3^{TG}$ mice.

P407 was injected into mice to induce HTG [24]. Serum triglycerides and triglyceride-rich lipoproteins were sharply elevated in $ApoC3^{TG}$ and P407-treated mice [24, 25]. When the plasma levels of triglycerides in P407-treated mice were comparable to those in $ApoC3^{TG}$ mice (~ 2000 mmol/dL, Supplementary Fig. 1C), the frequencies and activities of $CD8^+$ T^{P407} cells were determined. The frequencies of $CD8^+$ T, $CD8^+$ $NKG2D^+$ T, $CD8^+$ $CD44^+$ T, $CD8^+$ $CD44^+$ $KLRG1^+$ T, and $CD8^+$ $CD44^+$ $CD62L^-$ T decreased in the spleens of the P407-treated mice (Fig. 1F and Supplementary Fig. S1D–F). These $CD8^+$ T^{P407} cells had lower IFN-γ production rates (Fig. 1G), increased apoptosis rates (Fig. 1H and Supplementary Fig. S1G), and repressed proliferation (Fig. 1I). When the rest or IL-2-stimulated $CD8^+$ T cells of the WT mice were treated with various doses of P407 ex vivo, no changes in CD44 level (Supplementary Fig. S1H) or IFN-γ level were found in the $CD8^+$ T cells (Supplementary Fig. S1I), demonstrating that P407 was not toxic to $CD8^+$ T cells.

Given that ApoC3 was not expressed in the $CD8^+$ T cells of WT, TG, or P407 mice (Fig. 1J), the effects of cell-intrinsic ApoC3 on $CD8^+$ T cell function could be excluded. We

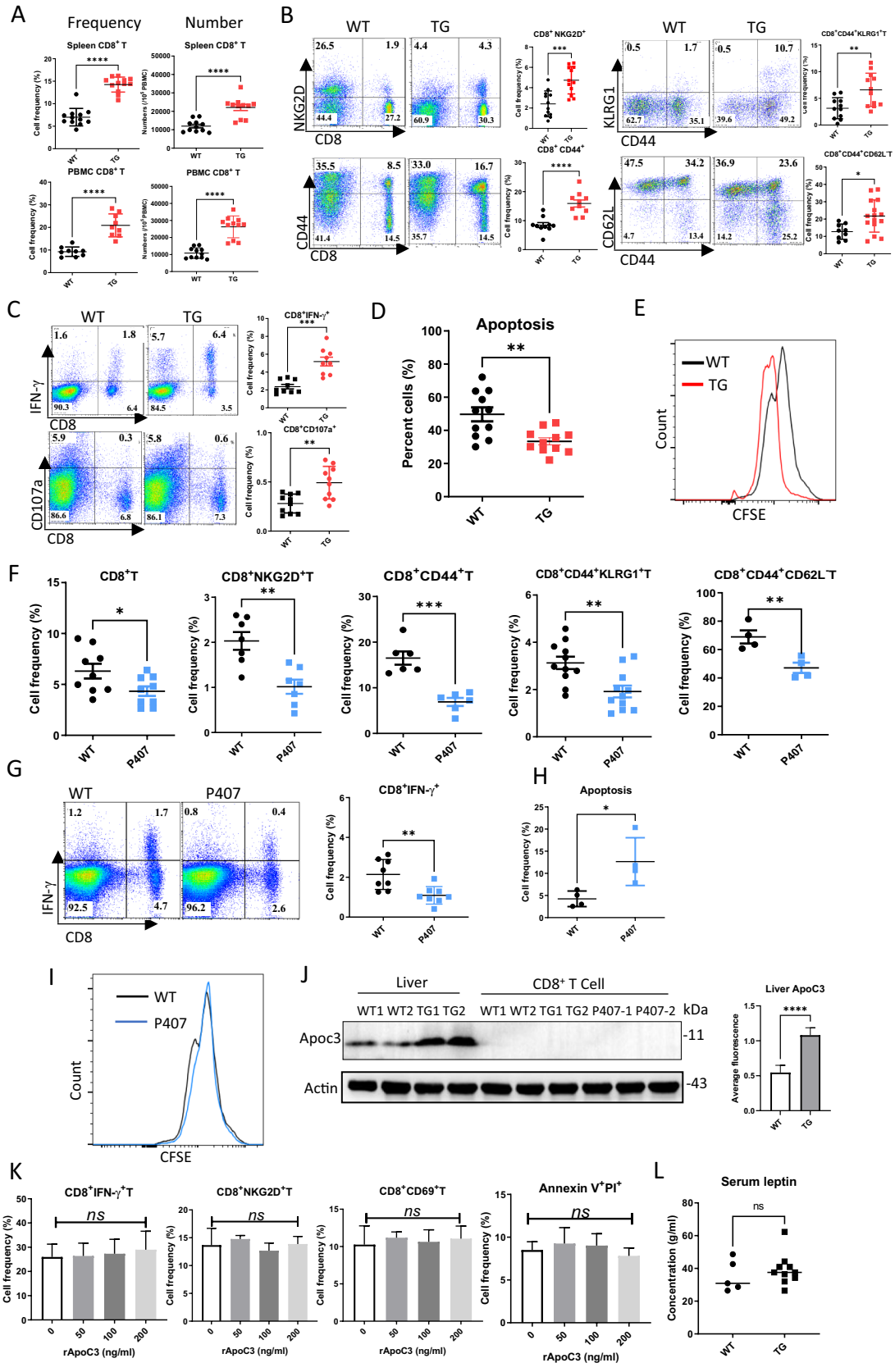
A
Frequency
Number
Spleen CD8+ T
PBMC CD8+ T
Cell frequency (%)
Numbers (/10^6 PBMC)
WT
TG
B
WT
TG
NKG2D
CD8
CD44
KLRG1
CD62L
CD8+ NKG2D+
CD8+ CD44+
CD8+CD44+KLRG1+T
CD8+CD44+CD62L-T
C
IFN-γ
CD107a
CD8+IFN-γ+
CD8+CD107a+
D
Apoptosis
Percent cells (%)
E
Count
CFSE
F
CD8+T
CD8+NKG2D+T
CD8+CD44+T
CD8+CD44+KLRG1+T
CD8+CD44+CD62L-T
Cell frequency (%)
P407
G
H
Apoptosis
I
Count
CFSE
J
Liver
CD8+ T Cell
WT1 WT2 TG1 TG2
WT1 WT2 TG1 TG2 P407-1 P407-2
kDa
Apoc3
Actin
-11
-43
Liver ApoC3
Average fluorescence
K
CD8+IFN-γ+T
CD8+NKG2D+T
CD8+CD69+T
Annexin V+PI+
ns
rApoC3 (ng/ml)
L
Serum leptin
Concentration (g/ml)

◂**Fig. 1** Increased $CD8^+$ T cell activities in $ApoC3^{TG}$ mice. **A** Detection of $CD8^+$ T cell frequencies and number in $ApoC3^{TG}$ mice. **B–C** Phenotypes, IFN-γ production and degranulation ($CD107a^+$) of $CD8^+$ T cells. **D–E** Apoptosis measured by Annexin V/PI and cell proliferation detected by CFSE dilution. **F** Frequencies and phenotypes of $CD8^+$ T cells of P407-treated mice. **G–I** IFN-γ production, apoptosis, and cell division in $CD8^+$ T^{P407} cells. **J** Detection of cell-intrinsic expression of ApoC3 in $CD8^+$ T cells. **K** Effects of recombinant Apoc3 on the activities of $CD8^+$ T cells. **L** Plasma leptin levels in $ApoC3^{TG}$ mice. Experiments were repeated twice. *Ns*, no significance. * $P<0.05$, ** $P<0.01$, and *** $P<0.001$

determined whether exogenous recombinant ApoC3 protein (rApoC3) affected $CD8^+$ T cell activities. After rApoC3 was incubated with $CD8^+$ T cells ex vivo, IFN-γ, NKG2D, and CD69 expression and apoptosis did not vary substantially (Fig. 1K and Supplementary Fig. S1J–K). Leptin is produced in obese individuals to stimulate $CD8^+$ T cells, and thus the plasma leptin levels of $ApoC3^{TG}$ mice were examined. No obvious changes were observed in the plasma leptin levels of $ApoC3^{TG}$ mice compared with those of WT mice (Fig. 1L). Therefore, increased bioactivities of $CD8^+$ T cells in $ApoC3^{TG}$ mice was not directly due to the stimulation by ApoC3.

Increased antitumor activity in $Apoc3^{TG}$ mice is dependent on the activation of $CD8^+$ T cells

We determined whether altered $CD8^+$ T cell activities in $ApoC3^{TG}$ mice affect tumor growth in vivo. After H-22 (hepatic cancer) or MC38 (colonic cancer) cells were subcutaneously injected into the back of each mouse, tumor growth in the $ApoC3^{TG}$ mice was remarkably repressed (Fig. 2A–B, D–E). Meanwhile, the growth of H-22 tumors or MC38 tumor was accelerated in P407 mice compared with those in the WT mice. The frequency of tumor-infiltrated $CD8^+$ T cell and expression of NKG2D or IFN-γ in the $CD8^+$ T cells substantially increased in the TG mice, whereas the frequencies of $CD8^+$, $CD8^+$ $NKG2D^+$ or $CD8^+$ IFN-γ^+ cells in the P407 mice either decreased or showed no change compared with those in the WT mice (Fig. 2C, F and Supplementary Fig. S2A, B, E). In the H-22-transplanted tumors, no difference in macrophage and DC distributions in cancerous tissues was found among the groups (Supplementary Fig. S2C), and no obvious polarization of tumor macrophages ($F4/80^+$ $CD86^+$, $F4/80^+$ $CD206^+$) was observed in tumor-bearing mice (Supplementary Fig. S2D).

The altered activities of antigen-specific $CD8^+$ T cells in $ApoC3^{TG}$ mice were further analyzed. B16F10 cells with the ectopic expression of ovalbumin (B16F10-OVA cells) were transplanted into mice, which were pre-immunized with ovalbumin protein (Fig. 2G). As expected, the TG mice had smaller melanomas than the WT mice, and the smallest tumors were observed in the TG mice with OVA pre-immunization (Fig. 2H–I). Notably, the frequencies of $CD8^+$ T, $CD8^+$ $CD44^+$ $KLRG1^+$ T, and $CD8^+$ $CD44^+$ $KLRG1^+$ OVA-tetramer$^+$ T cells increased in the OVA-pre-immunized TG mice (Fig. 2J and Supplementary Fig. S2F). When the $CD8^+$ T cells of mice with H-22 tumors were depleted (Fig. 2K), antitumor activity disappeared (Fig. 2L–M). The depletion of $CD8^+$ T cells in the tumor-bearing mice were verified (Fig. 2N and Supplementary Fig. S2G). Therefore, increased antitumor activity in $Apoc3^{TG}$ mice is dependent on the activation of $CD8^+$ T cells.

We explored the clinical significance of ApoC3 expression in patients with HCC by bioinformatics. According to the Cancer Genome Atlas (TCGA) data (https://www.cancer.gov/tcga), the ApoC3 expression levels of HCC tissues were substantially lower than those in paracancerous tissues (either paired or unpaired biopsies; Fig. 2O). Furthermore, ApoC3 expression in the HCC tissues decreased at the advanced T or N stages (Fig. 2P). High levels of ApoC3 in patients with HCC indicated increased survival (Fig. 2Q), and HCC patients with high ApoC3 levels had more cytotoxic cells (Fig. 2R) in the tumor microenvironment (TME). $CD8^+$ T cells constitute one of the two subsets of cytotoxic cells. The HCC biopsies of 49 patients were collected and used in determining the association of ApoC3 expression levels with $CD8^+$ T cells. In tumor tissue sections stained with ApoC3 or CD8 antibodies (Fig. 2S), ApoC3 expression was lower in the HCC tissue than in the paracarcinoma tissue. ApoC3 expression decreased at advanced TNM stages (Fig. 2T and Supplementary Fig. S2H). After the staining intensity of CD8 or ApoC3 in same section was half-quantified, Spearman's correlation coefficient was used for the analysis of ranked data. ApoC3 expression level in HCC was positively correlated with $CD8^+$ T cells in the TME (Fig. 2U). We demonstrated that high-ApoC3 individuals have increased antitumor activities involving $CD8^+$ T cells.

Palmitic acid downregulates $CD8^+$ T cell function ex vivo

Given the common features of high triglyceride and FFA levels in the plasma of $ApoC3^{TG}$ and P407-treated mice, palmitic acid (PA) was used to treat $CD8^+$ T cells ex vivo. After treatments with various doses of PA, IFN-γ production in the $CD8^+$ T cells substantially decreased (Fig. 3A and Supplementary Fig. S3A), while CD69 and NKG2D expression and the apoptosis of $CD8^+$ T cells did not vary remarkably (Fig. 3A and Supplementary Fig. S3A). We determined whether intake of FFAs and intracellular lipids of $CD8^+$ T cells increased in the $ApoC3^{TG}$ or P407-treated mice. We

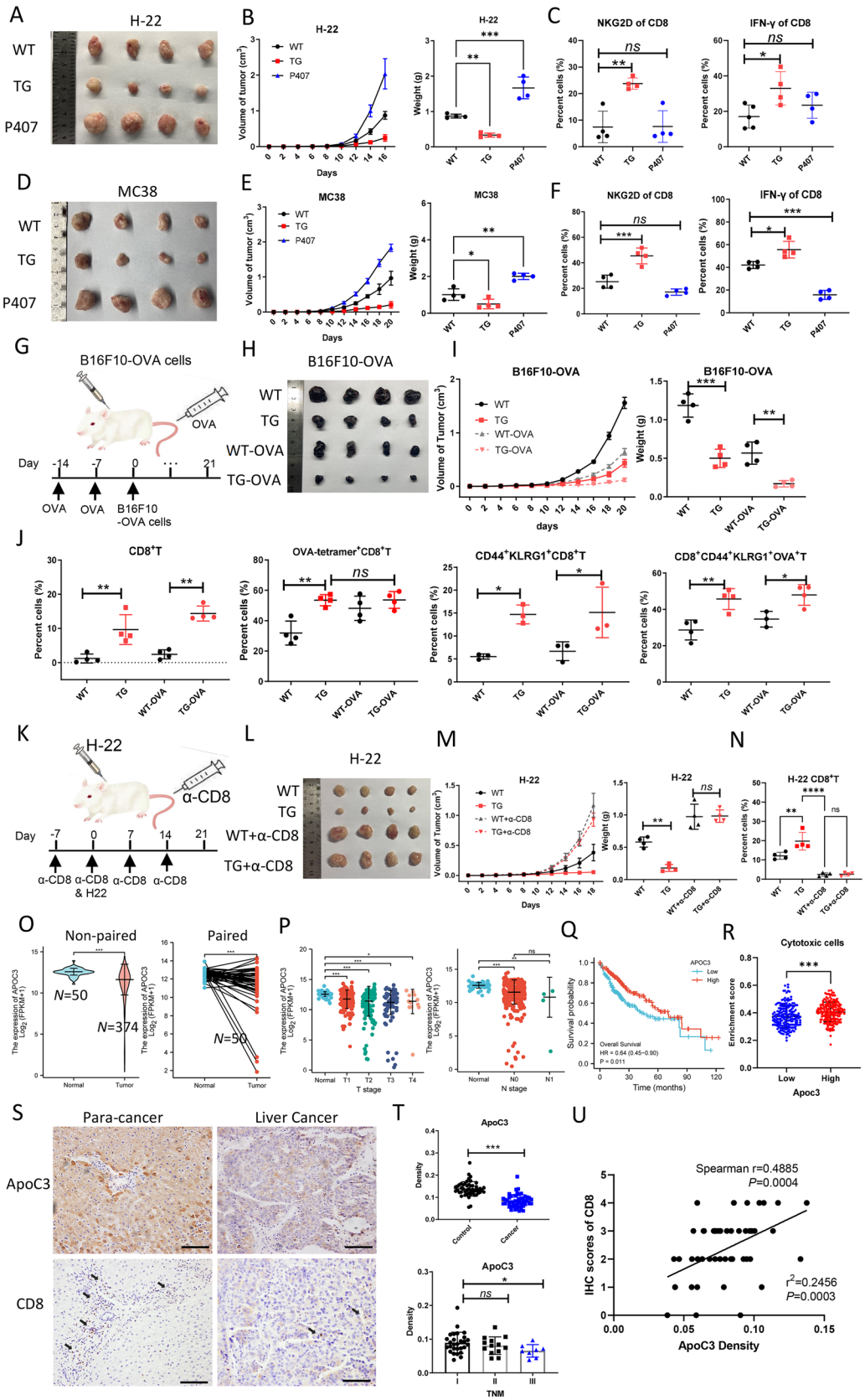
A
H-22
WT
TG
P407
B
H-22
WT
TG
P407
Volume of tumor (cm3)
Days
Weight (g)
C
NKG2D of CD8
IFN-γ of CD8
Percent cells (%)
D
MC38
E
MC38
F
NKG2D of CD8
IFN-γ of CD8
G
B16F10-OVA cells
OVA
Day -14 -7 0 ... 21
OVA OVA B16F10 -OVA cells
H
B16F10-OVA
WT-OVA
TG-OVA
I
B16F10-OVA
Volume of Tumor (cm3)
days
J
CD8+T
OVA-tetramer+CD8+T
CD44+KLRG1+CD8+T
CD8+CD44+KLRG1+OVA+T
K
H-22
α-CD8
Day -7 0 7 14 21
α-CD8 α-CD8 & H22 α-CD8 α-CD8
L
H-22
WT+α-CD8
TG+α-CD8
M
H-22
N
H-22 CD8+T
O
Non-paired
Paired
N=50
N=374
Normal
Tumor
P
T stage
Q
APOC3
Low
High
Overall Survival
HR = 0.64 (0.45–0.90)
P = 0.011
Survival probability
Time (months)
R
Cytotoxic cells
Enrichment score
Low
High
Apoc3
S
Para-cancer
Liver Cancer
ApoC3
CD8
T
ApoC3
Density
Control
Cancer
TNM
U
Spearman r=0.4885
P=0.0004
r2=0.2456
P=0.0003
IHC scores of CD8
ApoC3 Density

◂**Fig. 2** ApoC3 exerted antitumor activity involving $CD8^+$ T cells. **A** HCCs transplanted by subcutaneously injecting H-22 cells into mice. **B** Growth curves and weights of HCCs. **C** NKG2D or IFN-γ expression of tumor-infiltrated $CD8^+$ T cells detected by flow cytometry. **D** Transplanted colon cancer formed by MC38 cells in mice. **E** Growth curves and weights of colon cancer. **F** NKG2D or IFN-γ expression of tumor-infiltrated $CD8^+$ T cells detected by flow cytometry. **G–H** Melanoma formed by B16F10-OVA in WT or TG mice pre-primed with OVA protein. **I** Growth curves and weights of melanomas. **J** Frequencies of $CD8^+$, $CD8^+$ $CD44^+$ $KLRG1^+$, $CD8^+$ OVA-tetramer$^+$, and $CD8^+$ $CD44^+$ $KLRG1^+$ OVA-tetramer$^+$ cells in transplanted melanomas. **K–L** Transplanted HCCs in mice with depleted $CD8^+$ T cells. **M** Growth curves and weights of HCCs. **N** Loss of $CD8^+$ T cells in tumor tissues. **O** Based on TCGA analysis, the transcriptional levels of ApoC3 in patients with HCC. **P–R** Variations in ApoC3 expression levels among the T and N stages of HCC, survival probability, and the association with cytotoxic cell infiltration. **S–T** Staining HCC sections with ApoC3 and CD8 antibodies by IHC and density variations in ApoC3. **U** Correlational study on CD8 intensity with ApoC3 in HCC by Spearman rank correlation efficient and linear regression. Experiments were carried out twice. *Ns*, no significance. * $P<0.05$, ** $P<0.01$, and *** $P<0.001$

did not find changes in the levels of CD36 (Fig. 3B and Supplementary Fig. S3B) and intracellular FFAs (Fig. 3C) in $CD8^+$ T cells derived from $ApoC3^{TG}$ and P407-treated mice. The intensity of Nile red (staining of lipids) in $CD8^+$ T^{TG} cells was comparable to that in the $CD8^+$ T^{WT} cells, but lipid levels increased in the $CD8^+$ T^{P407} cells (Fig. 3D). Unexpectedly, PA treatment ex vivo did not affect CD36 expression in $CD8^+$ T cells even at a dose of 1200 μM (Fig. 3E and Supplementary Fig. S3A), although PA increases CD36 levels on NK cells [22]. When the $CD8^+$ T cells of CD36-deficient ($CD36^{-/-}$) mice were treated with PA, inhibition of IFN-γ was reduced (Fig. 3F and Supplementary Fig. S3C). Thus, although PA did not affect CD36 expression in the $CD8^+$ T cells, CD36-dependent intake of FFAs inhibited IFN-γ production. Finally, the heterozygotes of $ApoC3^{TG}$ mice crossed with $CD36^{-/-}$ mice were generated for the analysis of $CD8^+$ T cell activities. In the $ApoC3^{TG}$–$CD36^{\pm}$ mice, FFA intake by $CD8^+$ T cells were theoretically reduced by half. However, the frequencies and expression levels of NKG2D and IFN-γ did not decrease in the $CD8^+$ T cells (Fig. 3G), indicating that increased $CD8^+$ T cell activities in $ApoC3^{TG}$ mice were not involved with their intrinsic lipid metabolism.

Metabolic changes and RNA-seq profiles suggest $CD8^+$ T cell activation affected by surrounding cells

We determined whether changes in glycolipid metabolism affected $CD8^+$ T cell activities in the $ApoC3^{TG}$ or P407-treated mice. Under the same HTG microenvironment, $CD8^+$ T^{TG} cells unexpectedly promoted glycolysis and fatty acid synthesis, as indicated by increased levels of glucose receptor (GLUT1), hexokinase II (HK II), and ACC1 after stimulation by α-CD3/α-CD28 (Fig. 4A and Supplementary Fig. S4A). ECAR analysis confirmed enhanced glycolysis in the $CD8^+$ T^{TG} cells (Fig. 4B). Meanwhile, carnitine palmityltransferase 1 (CPT1), the key enzyme of fatty acid oxidation (FAO) was inhibited in physiologic $CD8^+$ T^{TG} cells, but with no changes were observed after $CD8^+$ T^{TG} cells were activated. Consistent with energy supplied by glycolysis in the $CD8^+$ T^{TG} cells, no changes in mitochondrial content and inhibited ROS production were observed in the mitochondria, indicating inhibited oxidative phosphorylation (Fig. 4C and Supplementary Fig. S4B). Mitochondrial content increased in the $CD8^+$ T^{P407} cells, indicating increase in the amount of energy supplied by the mitochondria in these $CD8^+$ T cells. No difference in cROS level was found among the three kinds of $CD8^+$ T cells.

mTOR is a key hub that regulates glycolysis [26]. Elevated levels of total mTOR, mTORC1, and S6 (a downstream signal of mTOR activation) were observed in the rest $CD8^+$ T^{TG} cells. Meanwhile, the expression of mTOR, p-mTOR, mTORC1, and p-S6 increased in the activated $CD8^+$ T^{TG} cells (Fig. 4D and Supplementary Fig. S4C). However, these signaling molecules had no obvious changes in the $CD8^+$ T^{P407} cells. The activation of mTOR is negatively regulated by the AMPK phosphorylation and positively regulated by Akt phosphorylation. As expected, although the total LKB1 and AMPK increased in the rest or activated $CD8^+$ T^{TG} cells, p-AMPK decreased in the $CD8^+$ T cells. Increases in total and phosphorylated Akt were observed in the activated $CD8^+$ T^{TG} cells (Fig. 4E and Supplementary Fig. S4D).

Consistent with mTOR activation, increases in the levels of SREBP1 and SREBP2 as key transcriptional factors in cellular synthesis of FFAs or cholesterol were observed in the activated $CD8^+$ T^{TG} cells (Fig. 4F and Supplementary Fig. S4E). We did not find obvious difference in PPAR-γ expression among the three kinds of $CD8^+$ T cells. In addition, the level of FOXO1, as a transcriptional factor regulated by Akt [27], increased in the $CD8^+$ T^{TG} cells (Fig. 4F). IFN-γ production was repressed when the $CD8^+$ T^{TG} cells were treated with an mTOR inhibitor (rapamycin) but increased when the cells were treated with an AMPK inhibitor (Compound C; Fig. 4G and Supplementary Fig. S4F–G). The inhibitors of Akt (Ly294002 or Wortmannin) decreased IFN-γ level in the $CD8^+$ T^{TG} cells (Fig. 4H and Supplementary Fig. S4H–I). Thus, enhanced glycolysis in the $CD8^+$ T^{TG} cells involved Akt/mTOR activation.

To determine molecular events leading to the activation of Akt/mTOR in the $CD8^+$ T^{TG} cells, we performed transcriptional sequencing, using $CD8^+$ T cells from the $ApoC3^{TG}$, P407-treated, and WT mice. A total of 791, 846, and 1438 differentially expressed genes (DEGs) were found

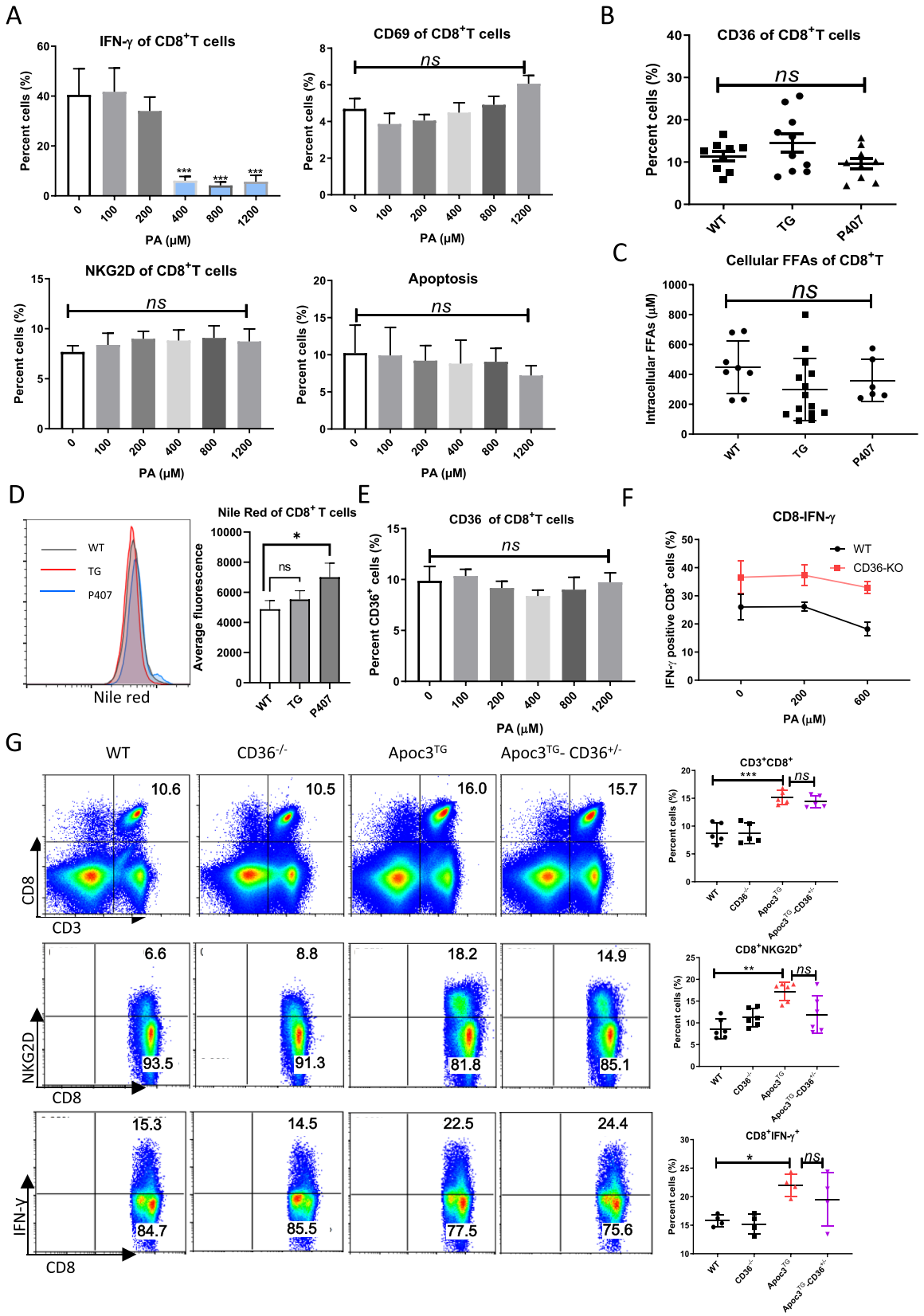
A
IFN-γ of CD8+T cells
Percent cells (%)
PA (μM)
CD69 of CD8+T cells
ns
NKG2D of CD8+T cells
Apoptosis
B
CD36 of CD8+T cells
WT
TG
P407
C
Cellular FFAs of CD8+T
Intracellular FFAs (μM)
D
Nile Red of CD8+ T cells
Average fluorescence
Nile red
E
CD36 of CD8+T cells
Percent CD36+ cells (%)
F
CD8-IFN-γ
IFN-γ positive CD8+ cells (%)
CD36-KO
G
WT
CD36-/-
Apoc3TG
Apoc3TG- CD36+/-
CD8
CD3
NKG2D
IFN-γ
10.6
10.5
16.0
15.7
6.6
8.8
18.2
14.9
93.5
91.3
81.8
85.1
15.3
14.5
22.5
24.4
84.7
85.5
77.5
75.6
CD3+CD8+
CD8+NKG2D+
CD8+IFN-γ+

◂**Fig. 3** Palmitic acid inhibits CD8$^+$T cell activation. **A** CD8$^+$ T cells were treated with various doses of palmitic acid (PA). **B**–**D** CD36, FFAs and droplets stained by Nile red of CD8$^+$ T cells from WT, TG, or P407-treated mice. **E** CD36 variations in CD8$^+$ T cells treated with PA ex vivo. **F** Comparison of IFN-γ production by CD8$^+$ T^{WT} and CD36$^{-/-}$-CD8$^+$ T cells after treatment with PA. **G** Detected frequencies of NKG2D and IFN-γ in CD8$^+$ T cells from WT, CD36$^{-/-}$, ApoC3^{TG}, or ApoC3^{TG}-CD36$^{\pm}$ mice. Experiments were repeated twice. *Ns*, no significance. * $P<0.05$, ** $P<0.01$, and *** $P<0.001$

between ApoC3^{TG} and P407 mice, P407 and WT mice, and ApoC3^{TG} and WT mice, respectively (Fig. 4I). The heatmaps of the DEGs in the three kinds of CD8$^+$ T cells are shown in Fig. 4J. KEGG analysis showed that the top 2 DEGs in TG versus WT or P407 were molecules involved in cell adhesion and cytokine and receptor interactions (Fig. 4K). Transcriptomics results suggested that the activation of CD8$^+$ T cell in Apoc3^{TG} mice were involved in contact with surrounding cells.

Antitumor activity of CD8$^+$ T cells in ApoC3^{TG} mice was regulated by macrophages

The activities of CD8$^+$ T cells are generally stimulated by DCs or macrophages in a cell-contact manner. The number of lipid-accumulating DCs with increased expression of inhibitory molecules (e.g., PD-L1 and TGF-β1) in the ApoC3^{TG} mice downregulate NK cell function [22]. ApoC3 stimulates an alternative mode of inflammasome activation in human macrophages but not in mouse macrophages [28]. Although no variations in the frequencies of macrophages were found among the mice (Supplementary Fig. S5A), macrophages^{TG} showed remarkable increase in the expression levels of CD86, NKG2D-ligand (NKG2DL), TNF-α, IL-1β, and IL-6, inhibited secretion of TGF-β1, and no changes in CD206, IL-10, PD-L1, and CD40 levels. By contrast, macrophages^{P407} showed decreased CD86, NKG2DL, IL-1β, IL-6, CD206, and TGF-β1 expression levels and maintained comparable TNF-α, IL-10, PD-L1, and CD40 expression levels, compared with macrophages^{WT} (Fig. 5A). Elevated cROS and mROS levels and mitochondrial content were observed in macrophages^{TG}, and moderate increase in cROS level was observed in macrophages^{P407} (Fig. 5B and Supplementary Fig. S5B).

We cocultured CD8$^+$ T cells with macrophages derived from different mice in vitro. Compared with macrophages^{WT}, macrophages^{TG} had remarkably upregulated CD8$^+$ T cells that express CD69 and IFN-γ and kill target cells but showed no change in NKG2D expression. By contrast, macrophages^{P407} had no effects on the cytotoxicity of CD8$^+$ T cells (Fig. 5C and Supplementary Fig. S5C) but decreased CD69 and NKG2D expression levels in the CD8$^+$ T cells. These results indicated that macrophages^{TG} upregulated the activities of CD8$^+$ T cells, whereas macrophages^{P407} suppressed the activation of the CD8$^+$ T cells. After CD8$^+$ T cells were cocultured with DC^{TG} or DC^{WT}, no variations in the CD69, CD44, IFN-γ, and NKG2D expression levels of CD8$^+$ T cells were found (Fig. 5D). Thus, the increased bioactivity of CD8$^+$ T^{TG} cell was affected by the stimulation of macrophages^{TG}.

Furthermore, we confirmed the stimulatory effect of macrophages by depleting macrophages in vivo with the peritoneal injection of clodronate. Decreases in macrophages in ascites and spleens were verified (Fig. 5E and Supplementary Fig. S5D). After liposome injection, peritoneal and splenic CD8$^+$ T^{TG} cells restored NKG2D expression. The frequencies of CD8$^+$ IFN-γ$^+$, CD8$^+$ CD107a$^+$, CD8$^+$ CD44$^+$, and CD8$^+$ CD44$^+$ KLRG1$^+$ cells in the ApoC3^{TG} mice decreased and returned to levels similar to those in CD8$^+$ T^{WT} cells (Fig. 5F and Supplementary Fig. S5E–F). Macrophages^{TG} or macrophages^{WT} were adoptively transferred to H-22-bearing mice. Tumor growth was repressed in mice with macrophages^{TG}, compared with that in mice with macrophages^{WT} (Fig. 5G–I). The infiltration of macrophages and CD8$^+$ T cells into tumor tissues was examined. Although more macrophages were distributed in the tumors of the ApoC3^{TG} mice, no obvious changes in macrophages in the tumors of WT-mice with macrophages^{TG} or macrophages^{WT} were observed (Fig. 5J and Supplementary Fig. S5G). However, the frequencies of CD8$^+$ NKG2D$^+$, CD8$^+$ IFN-γ$^+$, CD8$^+$ CD44$^+$, and CD8$^+$ CD44$^+$ KLRG1$^+$ cells increased in the tumors of mice with macrophages^{TG} despite that CD8$^+$ T cell frequency did not vary (Fig. 5K and Supplementary Fig. S5H). These results demonstrated that activated macrophages in the ApoC3^{TG} mice stimulated CD8$^+$ T cells to suppress tumor growth in vivo.

PLA2/NOX2-induced alternative inflammasome activation in macrophages^{TG}

The molecular mechanisms of macrophage activation in ApoC3^{TG} mice were investigated by performing transcriptome sequencing on macrophages from the three kinds of mice. A total of 656, 1899, and 2638 DEGs were found between Apoc3^{TG} and WT mice, WT and P407-treated mice, and ApoC3^{TG} and P407-treated mice, respectively (Fig. 6A). Among the DEGs of the TG versus WT comparison, the top 2 variated genes were involved in cell adhesion and arachidonic acid metabolism. In the DEGs in the TG versus P407 comparison, most changed genes were involved with inflammation (e.g., cytokine and cytokine receptor interaction, TNF signaling, NF-κB signaling, and MAPK signaling; Supplementary Fig. S6A). We sorted out DEGs that

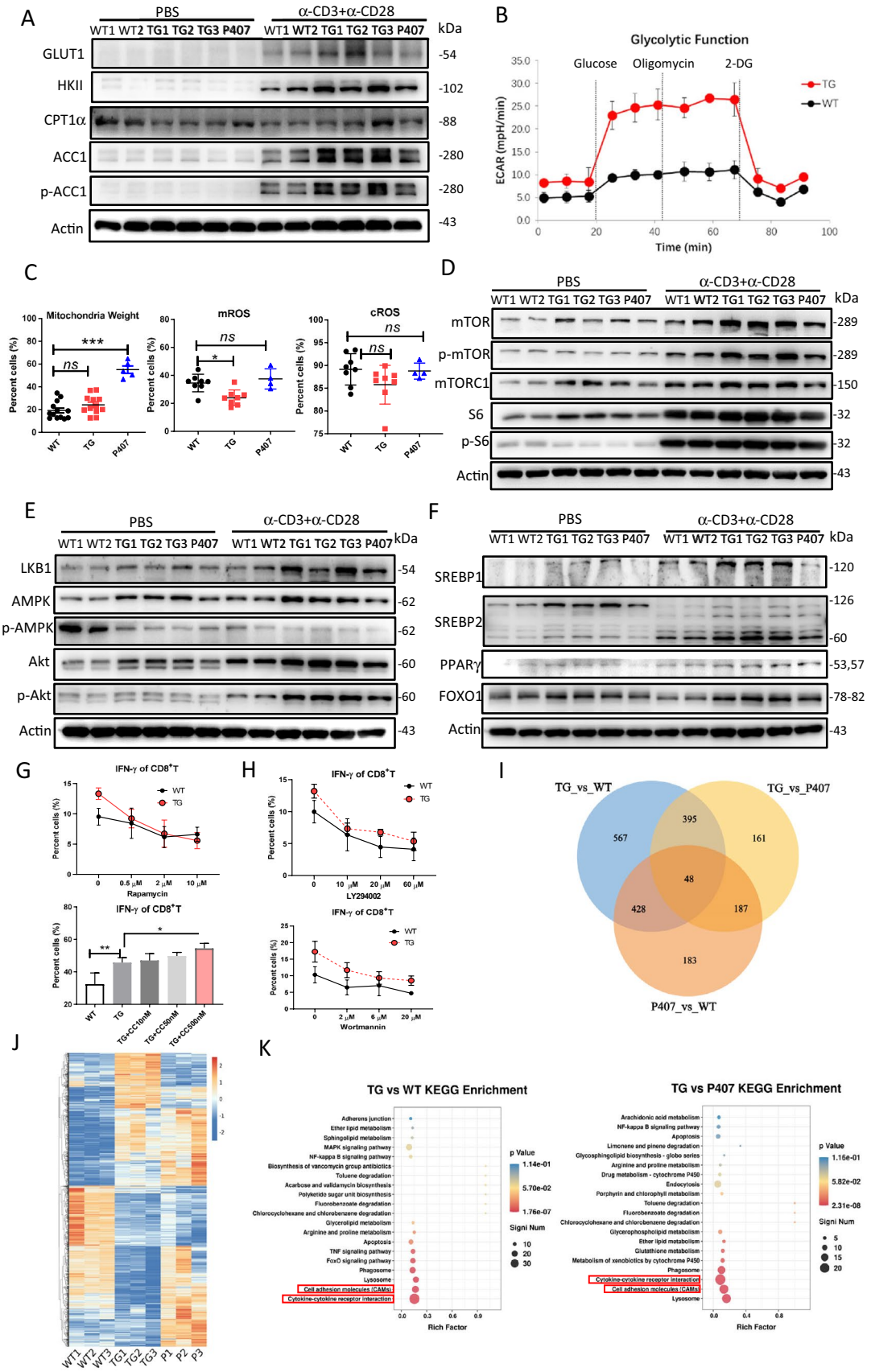
A
PBS
α-CD3+α-CD28
WT1 WT2 TG1 TG2 TG3 P407
WT1 WT2 TG1 TG2 TG3 P407
kDa
GLUT1
HKII
CPT1α
ACC1
p-ACC1
Actin
-54
-102
-88
-280
-280
-43
B
Glycolytic Function
Glucose
Oligomycin
2-DG
TG
WT
ECAR (mpH/min)
Time (min)
C
Mitochondria Weight
mROS
cROS
Percent cells (%)
ns
***
*
WT
TG
P407
D
PBS
α-CD3+α-CD28
WT1 WT2 TG1 TG2 TG3 P407
WT1 WT2 TG1 TG2 TG3 P407
kDa
mTOR
p-mTOR
mTORC1
S6
p-S6
Actin
-289
-289
-150
-32
-32
-43
E
PBS
α-CD3+α-CD28
WT1 WT2 TG1 TG2 TG3 P407
WT1 WT2 TG1 TG2 TG3 P407
kDa
LKB1
AMPK
p-AMPK
Akt
p-Akt
Actin
-54
-62
-62
-60
-60
-43
F
PBS
α-CD3+α-CD28
WT1 WT2 TG1 TG2 TG3 P407
WT1 WT2 TG1 TG2 TG3 P407
kDa
SREBP1
SREBP2
PPARγ
FOXO1
Actin
-120
-126
-60
-53,57
-78-82
-43
G
IFN-γ of CD8+T
Percent cells (%)
WT
TG
Rapamycin
IFN-γ of CD8+T
Percent cells (%)
**
*
WT
TG
TG+CC10nM
TG+CC50nM
TG+CC500nM
H
IFN-γ of CD8+T
Percent cells (%)
WT
TG
LY294002
IFN-γ of CD8+T
Percent cells (%)
WT
TG
Wortmannin
I
TG_vs_WT
TG_vs_P407
P407_vs_WT
567
395
161
48
428
187
183
J
WT1
WT2
WT3
TG1
TG2
TG3
P1
P2
P3
K
TG vs WT KEGG Enrichment
Adherens junction
Ether lipid metabolism
Sphingolipid metabolism
MAPK signaling pathway
NF-kappa B signaling pathway
Biosynthesis of vancomycin group antibiotics
Toluene degradation
Acarbose and validamycin biosynthesis
Polyketide sugar unit biosynthesis
Fluorobenzoate degradation
Chlorocyclohexane and chlorobenzene degradation
Glycerolipid metabolism
Arginine and proline metabolism
Apoptosis
TNF signaling pathway
FoxO signaling pathway
Phagosome
Lysosome
Cell adhesion molecules (CAMs)
Cytokine-cytokine receptor interaction
p Value
1.14e-01
5.70e-02
1.76e-07
Signi Num
10
20
30
Rich Factor
TG vs P407 KEGG Enrichment
Arachidonic acid metabolism
NF-kappa B signaling pathway
Apoptosis
Limonene and pinene degradation
Glycosphingolipid biosynthesis - globo series
Arginine and proline metabolism
Drug metabolism - cytochrome P450
Endocytosis
Porphyrin and chlorophyll metabolism
Toluene degradation
Fluorobenzoate degradation
Chlorocyclohexane and chlorobenzene degradation
Glycerophospholipid metabolism
Ether lipid metabolism
Glutathione metabolism
Metabolism of xenobiotics by cytochrome P450
Phagosome
Cytokine-cytokine receptor interaction
Cell adhesion molecules (CAMs)
Lysosome
p Value
1.16e-01
5.82e-02
2.31e-08
Signi Num
5
10
15
20
Rich Factor

◂**Fig. 4** Metabolic changes and RNA-Seq of $CD8^+$ T^{TG} cells. **A** Levels of Glut1, HK II, CPT1, and ACC1/p-ACC1 in $CD8^+$ T^{WT}, $CD8^+$ T^{TG}, and $CD8^+$ T^{P407} in the Western blot results. **B** Detection of ECAR. **C** Mitochondrial content and mROS, and cROS levels measured by flow cytometry. **D–F** Factors involved in glycolipid metabolism, such as mTOR, S6, LKB1, AMPK, Akt, SREBP1/2, PPARγ, and FOXO1 levels of $CD8^+$ T cells. **G–H** Inhibition of mTOR (rapamycin), AMPK (compound C) and Akt (LY294002, wortmannin) on the IFN-γ production of $CD8^+$ T cells. **I** DEGs between $CD8^+$ T cells of indicated mice. **J** Heatmap of DEGs. **K** Top different signaling pathways analyzed by KEGG. Experiments were repeated twice. *Ns*, no significance. * $P<0.05$, ** $P<0.01$, and *** $P<0.001$

were highly transcribed in $macrophages^{TG}$ and those with decreased transcription levels in $macrophages^{P407}$ simultaneously. The DEGs are listed in Fig. 6B. Most changed genes in arachidonic acid metabolism are listed in Fig. 6C, including PLA2 (the key enzyme in arachidonic acid metabolism). Western blot results confirmed the increased expression of cytosolic PLA2 components, including PLA2 G4A and PLA2 G4F, but not the secreted PLA2 G2D in $macrophages^{TG}$. No changes were found in $macrophages^{P407}$ (Fig. 6D and Supplementary Fig. S6B). Given that NOX2 in macrophages is activated by cPLA2 [29], NOX2 level also increased (Fig. 6D and Supplementary Fig. S6B).

NOX2-induced ROS production contributes to alternative inflammasome activation in human monocytes stimulated by ApoC3 [28]. $Macrophages^{TG}$ increased cROS production (Fig. 5B). DEGs involved in the alternative inflammasome activation of macrophages are shown in Fig. 6E. Multiple genes, including *TLR2*, *TRPM2*, *TXNIP*, *PYCARD*, *CASP1*, *CASP8*, *SYK*, and *LYN*, showed increased transcription levels in $macrophages^{TG}$ but decreased transcription levels in $macrophages^{P407}$. The protein levels of ASC, NLRP3, RIPK1, c-Cas8, c-Cas1, c-IL-1β, and c-GSDMD all increased in $macrophages^{TG}$, but had no obvious changes in $macrophages^{P407}$ (Fig. 6F and Supplementary Fig. S6C). The release of LDH was also increased in $macrophages^{TG}$ (Fig. 6G). When the activation of Cas8, Cas1, or NLRP3 was blocked by their respective inhibitors (Z-IETD-FMK, Z-YVAD-FMK, or MCC950), intracellular IL-1β (Fig. 6H and Supplementary Fig. S6D–F) and IL-1β (Fig. 6I) secretion was suppressed. These results demonstrated that the macrophages of $ApoC3^{TG}$ mice promoted pyroptosis by upregulating the activation of inflammasomes.

To determine whether NLRP3/Cas1 inflammasome activation in $macrophages^{TG}$ depends on cellular ROS, we added *N*-acetyl-*L*-cysteine (NAC) as an antioxidant to macrophages. Although ASC expression did not vary after NAC treatment, the expression levels of NLRP3, RIPK1, c-Cas8, and c-Cas1 in $macrophages^{TG}$ substantially decreased (Fig. 6J and Supplementary Fig. S6G). The production of intracellular IL-1β in $macrophages^{TG}$ was inhibited (Fig. 6K and Supplementary Fig. S6H), and IL-1β secretion in the supernatants of the rest and LPS/nigerin-stimulated $macrophages^{TG}$ was restored after NAC treatment (Fig. 6L). When $macrophages^{TG}$ were pretreated with NAC, their stimulatory capacities for the NKG2D and IFN-γ expression of $CD8^+$ T cells disappeared (Fig. 6M and Supplementary Fig. S6I).

To verify that increase in NOX2 level in $macrophages^{TG}$ was due to PLA2 activation, we used an inhibitor (CAY10650) of cPLA2. When the macrophages of the $Apoc3^{TG}$ mice were treated with CAY10650, the levels of NOX2, NLRP3, and GSDMD in $macrophages^{TG}$ substantially decreased, demonstrating that NOX2 was stimulated by PLA2 activation (Fig. 6N and Supplementary Fig. S6J). Notably, $macrophages^{TG}$ showed decreased CPT1α expression after CAY10650 treatment, indicating that cPLA2 affected cell-intrinsic fatty acid oxidation (Fig. 6N and Supplementary Fig. S6J). Furthermore, cPLA2 inhibitor (CAY10650), rather than secreted PLA2 inhibitor (Varespladid), inhibited production (Fig. 6O and Supplementary Fig. S6K-L) and release of IL-1β by $macrophages^{TG}$ under a rest or activated microenvironment (Fig. 6P). Collectively, these results showed that ROS production for the inflammasome activation of macrophages was induced by the cPLA2/NOX2 axis in the $Apoc3^{TG}$ mice.

ApoC3 stimulates Syk/cPLA2 to activate inflammasomes in macrophages

Given that Syk and Lyn are coupled with the cytoplasmic tail of TLR2 or TLR4 [30] and RNA-seq results indicated increased Syk and Lyn expression in $macrophages^{TG}$, we determined whether ApoC3 can directly ligate with TLR2/TLR4 to induce Syk phosphorylation. After the increased Apoc3 expression of macrophages was confirmed in the $ApoC3^{TG}$ mice, elevated levels of Syk, p-Syk, and CCDC109A (a calcium channel of mitochondria as an activation marker) increased in $macrophages^{TG}$ (Fig. 7A and Supplementary Fig. S7A). ApoC3 is identified as an endogenous mediator that led to Syk activation in human monocytes by binding membrane heterodimer of TLR2 and TLR4 [28]. ApoC3, TLR2, TLR4 and Syk sequences and structures of mouse and human are highly homologous, and the highly similar sequences of intracellular domains of TLR2 and TLR4 lead to highly conserved TLR signaling systems between species [31–33]. The ligation of ApoC3 with TLR2 was promoted in $macrophages^{TG}$ in the confocal images (Fig. 7B). Bright p-Syk staining was observed in $macrophages^{TG}$, and the increased overlay of TLR2 and p-Syk of $macrophages^{TG}$ (Fig. 7C) indicated that ApoC3 ligated with TLR2 to induce Syk activation. The cell membrane TLR2/TLR4 of $macrophages^{TG}$ was detected by flow cytometry. Higher TLR4 levels were observed in the cell

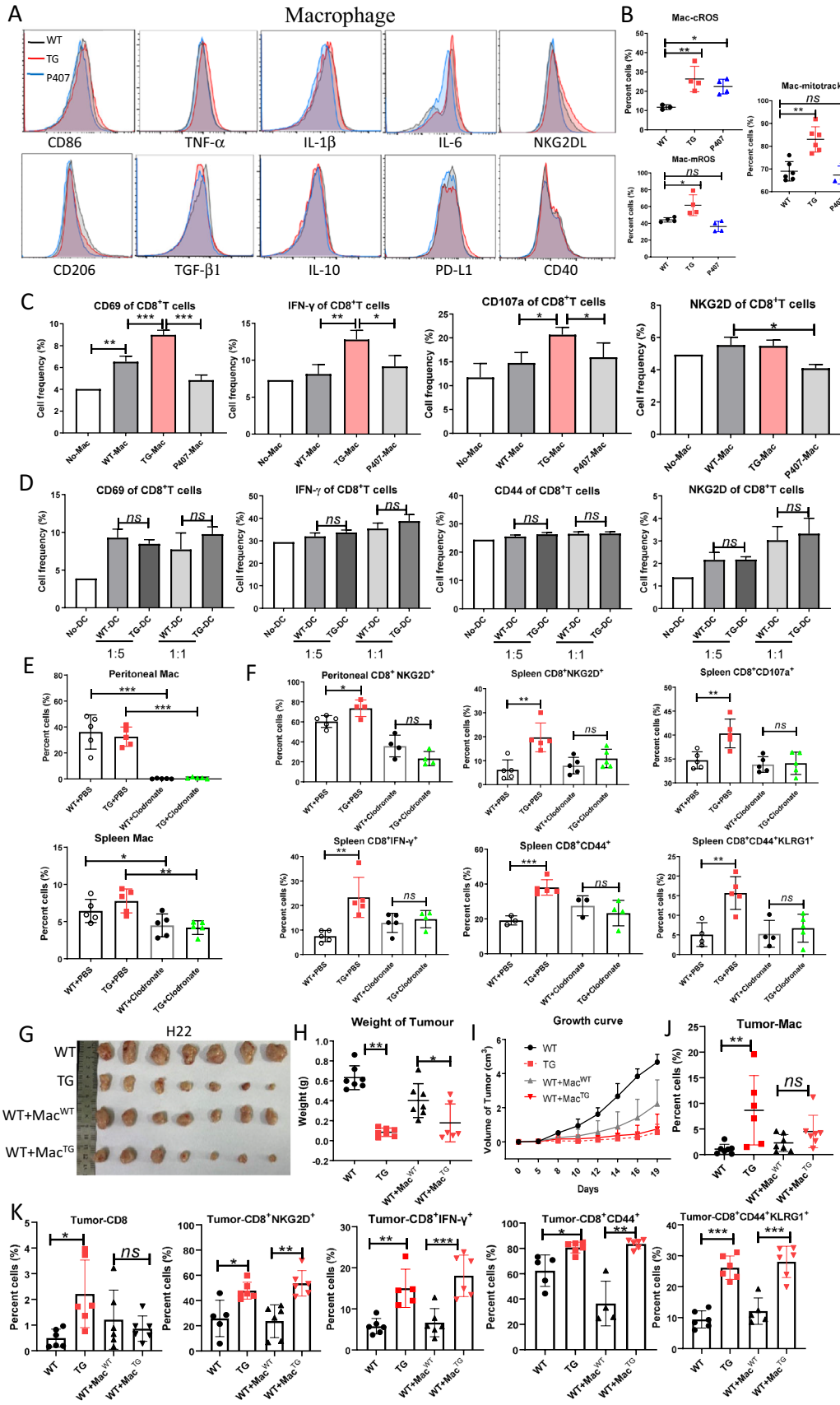
A
Macrophage
WT
TG
P407
CD86
TNF-α
IL-1β
IL-6
NKG2DL
CD206
TGF-β1
IL-10
PD-L1
CD40
B
Mac-cROS
Mac-mitotracker
Mac-mROS
Percent cells (%)
C
CD69 of CD8+T cells
IFN-γ of CD8+T cells
CD107a of CD8+T cells
NKG2D of CD8+T cells
Cell frequency (%)
No-Mac
WT-Mac
TG-Mac
P407-Mac
D
CD69 of CD8+T cells
IFN-γ of CD8+T cells
CD44 of CD8+T cells
NKG2D of CD8+T cells
No-DC
WT-DC
TG-DC
1:5
1:1
E
Peritoneal Mac
Spleen Mac
WT+PBS
TG+PBS
WT+Clodronate
TG+Clodronate
F
Peritoneal CD8+ NKG2D+
Spleen CD8+NKG2D+
Spleen CD8+CD107a+
Spleen CD8+IFN-γ+
Spleen CD8+CD44+
Spleen CD8+CD44+KLRG1+
G
H22
WT
TG
WT+MacWT
WT+MacTG
H
Weight of Tumour
Weight (g)
I
Growth curve
Volume of Tumor (cm3)
Days
J
Tumor-Mac
K
Tumor-CD8
Tumor-CD8+NKG2D+
Tumor-CD8+IFN-γ+
Tumor-CD8+CD44+
Tumor-CD8+CD44+KLRG1+

◂**Fig. 5** Macrophage in Apoc3^{TG} mice contribute to CD8^{+} T cell activation. **A** Phenotype and cytokine production of macrophages detected by flow cytometry. **B** Mitochondrial content and mROS and cROS levels in the macrophages of indicated mice. **C**–**D** After CD8^{+} T cells were cocultured with macrophages and DCs from ApoC3^{TG} mice, CD8^{+} T cell activation was determined. **E** Macrophages in mice after treatment with Clodronate. **F** Detection of CD8^{+} T cell activities in ApoC3^{TG} mice treated with Clodronate. **G** Growth of HCC in mice with adoptively transfer of macrophages^{WT} or macrophages^{TG}. **H**–**K** Tumor size, weight, growth curve, tumor-infiltrated macrophages, and CD8^{+} T cells. Experiments were repeated twice. *Ns*, no significance. * $P<0.05$, ** $P<0.01$, and *** $P<0.001$

membranes in macrophages^{TG}, but no changes in TLR2 level was found (Fig. 7D and Supplementary Fig. S7B).

To verify the contribution of Syk to inflammasome activation, we added R406, as an inhibitor of Syk phosphorylation, to treat macrophages^{TG}. The macrophages of ApoC3^{TG} mice showed decreased IL-1β production and secretion after R406 treatment (Fig. 7E and Supplementary Fig. S7C). R406 efficiently inhibited the cytoplasmic ROS production of macrophages^{TG} but weakly inhibited mitochondrial ROS production (Fig. 7F and Supplementary Fig. S7D). Syk activation only mildly affected oxidative phosphorylation in the mitochondria of macrophages^{TG}. R406 treatment decreased the expression levels of cPLA2, NOX2, RIPK1, c-Cas8, NLRP3, c-Cas1, and c-GSDMD (Fig. 7G and Supplementary Fig. S7E) and inhibited the release of LDH (Fig. 7H). Thus, Syk activation was a key signaling event in the alternative inflammasome activation of macrophages in the ApoC3^{TG} mice.

The NLRP3 inflammasome is activated in a two-signal process [34]. First, a signal mediates a priming step and NF-κB or MAPK signaling is induced through the PAMP- or DAMP-mediated activation of TLR4 or TNFR. As a result of NF-κB or MAPK activation, expressions of NLRP3, pro-IL-1β, and pro-IL-18 proteins increase. A second signal (potassium efflux, calcium influx, or cellular or mitochondrial ROS) mediates inflammasome assembly and Cas1 activation. We determined whether Syk activation can provide double signals for NLRP3 inflammasome activation. As shown in Fig. 7I and Supplementary Fig. S7F, the PI3K/Akt, NF-κB, and MAPK (Erk/Jnk/p38) signaling pathways were upregulated in macrophages^{TG}. When the macrophages of ApoC3 were treated with R406, the signaling molecules restored the expression levels (Fig. 7J and Supplementary Fig. S7F). Syk activation induced the activation of NOX2 by TRPM2 (a calcium channel of cell memebrane) [28]. When flufenamic acid, as a blocker of TRPM2, was used to treat macrophages^{TG}, cROS production (Fig. 7K and Supplementary Fig. S7G) and IL-1β production (Fig. 7L and Supplementary Fig. S7H), and IL-1β secretion (Fig. 7M) all decreased, indicating that TRPM2 was involved in Syk-induced alternative mode of inflammasome activation.

Subsidiarity of FAO-induced inflammasome activation in macrophages^{TG}

Given the typical feature of high triglyceride and FFA levels in the plasma of ApoC3^{TG} mice, whether macrophages^{TG} increased the intake of triglyceride-related proteins and FFAs to affect their inflammatory activities were investigated. Compared with macrophages^{WT}, macrophages^{TG} and macrophages^{P407} showed increased scavenger receptor (CD204) expression, but macrophages^{TG} had the highest levels of CD204 (Fig. 8A and Supplementary Fig. S8A). Elevated CD36 expression was observed in macrophages^{TG} but not in macrophages^{P407} (Fig. 8B and Supplementary Fig. S8B). Lipid droplets accumulated in macrophages^{TG}, as demonstrated in the confocal images (Fig. 8C) and flow-cytometric results (Fig. 8D). Consistent with CD36 expression, intracellular FFA level increased in macrophages^{TG} (Fig. 8E). PA stimulation (200 μM) can directly upregulate CD36 expression in macrophages (Supplementary Fig. S8C). When the glycolipid metabolism of macrophages^{TG} was checked, the expression levels of HK II and CPT1α increased (Fig. 8F and Supplementary Fig. S8D). ECAR and OCR analyses confirmed enhanced glycolysis (Fig. 8G) and oxidative phosphorylation (Fig. 8H), indicating macrophages^{TG} increased FAO. Elevated OCR and FAO in macrophages^{TG} may explain the increase in mROS level in macrophages^{TG} (Fig. 5B).

We then determined whether increased intake of lipids by macrophages^{TG} can critically affect the classical NLRP3-inflammasome activation. The macrophages of ApoC3^{TG}–CD36$^{\pm}$ mice did not show any changes in IL-1β, TNF-α, and IL-6 production (Fig. 8I and Supplementary Fig. S8F) and CD86, NKG2DL, and RAE-1 expression (Supplementary Fig. S8E), compared with those in the ApoC3^{TG} mice. Similarly, macrophages from heterozygous mice had comparable mitochondrial content, and cROS and mROS levels (Fig. 8J and Supplementary Fig. S8G). These results suggested that FFA intake was not a key factor for inflammasome activation. Moreover, we did not observe obvious changes in the levels of ATGL and CGI58, as key enzymes in lipolysis, in the macrophages from three kinds of mice (Fig. 8K and Supplementary Fig. S8H).

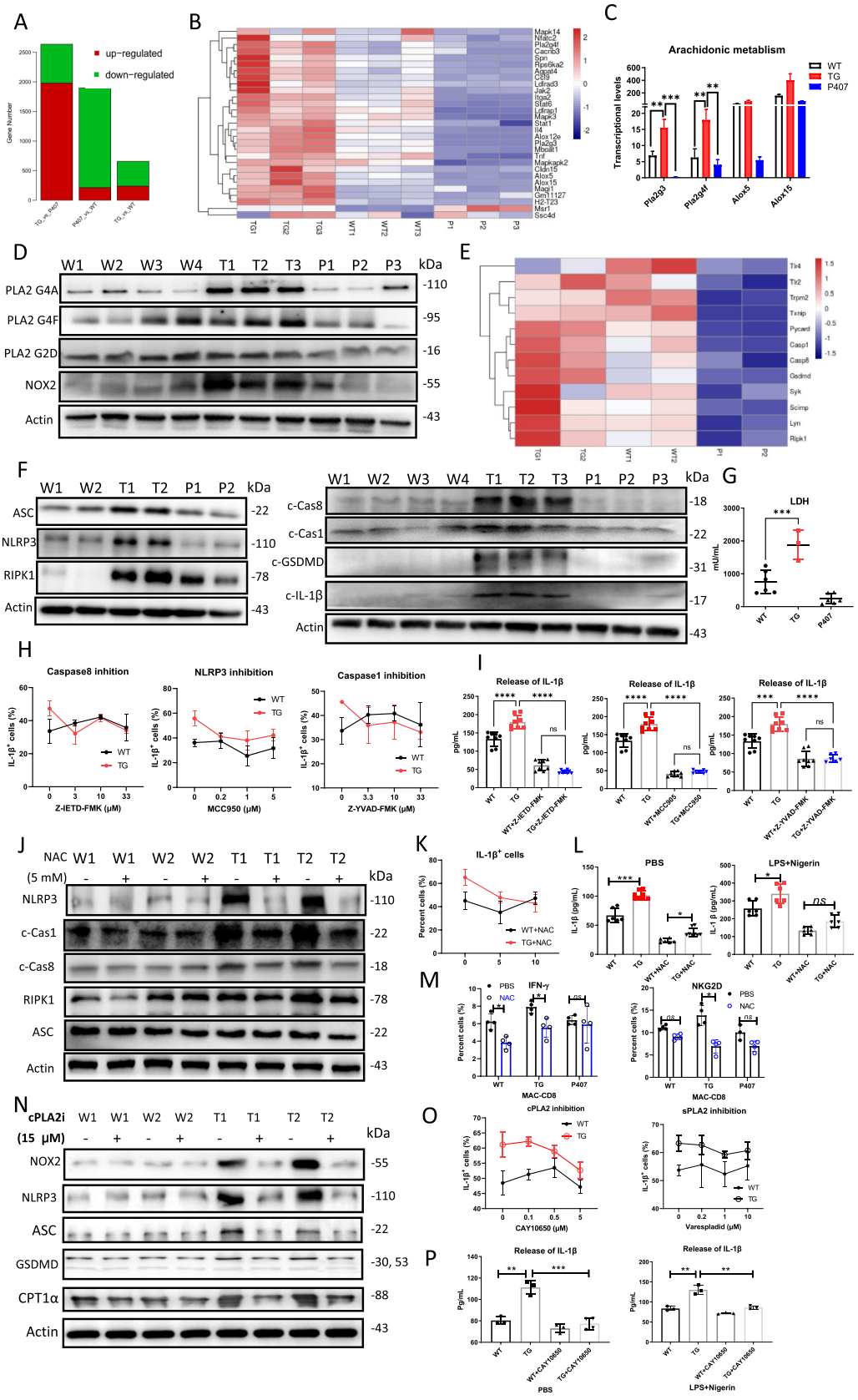
A
up−regulated
down−regulated
Gene Number
B
C
Arachidonic metablism
WT
TG
P407
Transcriptional levels
Pla2g3
Pla2g4f
Alox5
Alox15
D
W1 W2 W3 W4 T1 T2 T3 P1 P2 P3 kDa
PLA2 G4A -110
PLA2 G4F -95
PLA2 G2D -16
NOX2 -55
Actin -43
E
F
W1 W2 T1 T2 P1 P2 kDa
ASC -22
NLRP3 -110
RIPK1 -78
Actin -43
W1 W2 W3 W4 T1 T2 T3 P1 P2 P3 kDa
c-Cas8 -18
c-Cas1 -22
c-GSDMD -31
c-IL-1β -17
Actin -43
G
LDH
mU/mL
H
Caspase8 inhition
NLRP3 inhibition
Caspase1 inhibition
IL-1β+ cells (%)
Z-IETD-FMK (μM)
MCC950 (μM)
Z-YVAD-FMK (μM)
I
Release of IL-1β
pg/mL
J
NAC (5 mM)
W1 W1 W2 W2 T1 T1 T2 T2 kDa
NLRP3 -110
c-Cas1 -22
c-Cas8 -18
RIPK1 -78
ASC -22
Actin -43
K
IL-1β+ cells
Percent cells (%)
WT+NAC
TG+NAC
L
PBS
LPS+Nigerin
IL-1β (pg/mL)
M
IFN-γ
NKG2D
PBS
NAC
MAC-CD8
N
cPLA2i (15 μM)
W1 W1 W2 W2 T1 T1 T2 T2 kDa
NOX2 -55
NLRP3 -110
ASC -22
GSDMD -30, 53
CPT1α -88
Actin -43
O
cPLA2 inhibition
sPLA2 inhibition
CAY10650 (μM)
Varespladid (μM)
P
Release of IL-1β
Pg/mL
PBS
LPS+Nigerin

◂**Fig. 6** PLA2/NOX-induced inflammasome activation in macrophages^{TG}. **A** DEGs of macrophages by pairwise comparison. **B** Multiple genes that were upregulated in macrophages^{TG} whereas downregulated in macrophages^{TG} were sorted out. **C** Genes that were associated with arachidonic acid metabolism and had the most changes. **D** Western blot confirmed elevated expression of PLA2 G4A/G4F and NOX2 in macrophages^{TG}. **E** Transcriptional variations in genes associated with alternative inflammasome activation. **F** Confirmed alternative inflammasome activation by Western blot. **G** Upregulated pyroptosis of macrophages^{TG} identified by LDH releasing assay. **H–I** Inhibition of Cas8, NLRP3, or Cas1 decreased IL-1β production or secretion of macrophages^{TG}. **J** NAC was used to deplete cellular ROS, and NAC treatment decreased NLRP3, c-Cas1, c-Cac8, and RIPK1 protein levels. **K–L** IL-1β production or secretion by the NAC treatment. **M** Macrophages^{TG} lost stimulatory effects on CD8$^+$ T cells after ROS depletion. **N** Inhibited cPLA2 (CAY10650) on NOX2, inflammasome activation, and CPT1 expression in macrophages^{TG}. **O** IL-1β production of macrophages^{TG} treated with CAY10650 or a sPLA2 inhibitor (Varespladid). **P** Release of IL-1β by rest or activated macrophages^{TG} after treatment with CAY10650. Experiments were repeated twice. *Ns*, no significance. * $P<0.05$, ** $P<0.01$, and *** $P<0.001$

This result indicated that FFAs derived from triglyceride hydrolysis did not affect inflammasome activation. However, when macrophages^{TG} was treated with the inhibitor of cPLA2 (CAY10650) or Syk (R406), basal respiration substantially recovered (Fig. 8L). FFAs that mediate FAO in macrophages^{TG} were mainly derived from phospholipid hydrolysis because of cPLA2 activation.

Next, we analyzed the effects of FAO inhibition with a CPT1α inbitor (etomoxir) on inflammasome activation in macrophages^{TG}. As shown in Fig. 8M and Supplementary Fig. 8SI, treatment with etomoxir mildly decreased IL-1β production and release by macrophages^{TG}. Given that oxidative phosphorylation in the mitochondria always generates ROS, macrophages^{TG} further depleted mROS with TEMPO. Although IL-1β production was not affected, IL-1β secretion was decreased by macrophages^{TG} (Fig. 8N and Supplementary Fig. 8SJ–K), indicating that mROS contributed to the signal 2 activation of inflammasomes. Finally, we stimulated macrophages^{WT} with rApoC3, PA, or rApoC3/PA to observe their inflammasome activation ex vivo. Cotreatment with rApoC3 and PA led to the highest rates of c-Cas1, c-GSDMD, and c-IL-1β production. rApoC3 alone stimulated p-Syk, c-Cas8, NLRP3, c-Cas1, c-GSDMD, pro-IL-1β, and c-IL-1β expression, and PA alone weakly increased p-Syk, c-Cas8, c-GSDMD, and pro-IL-1β expression (Fig. 8O). The inflammatory activities of macrophages^{TG} can be attributed to Syk/cPLA2 activation, which not only stimulates the alternative inflammasome through the cROS/RIPK1/c-Cas8/c-Cas1 signaling axis but also induces classical inflammasome activation by the FAO-induced mROS/c-Cas1 axis. However, the alternative pathway plays a major role, whereas the classical pathway plays a minor role.

Discussion

Increased prevalence of cancer in obese individuals is generally related to immune depression induced by hyperlipidemia. However, we demonstrated that ApoC3 exerts protective effects against tumor progression by increasing CD8$^+$ T cell activity through inflammasome activation of macrophages in ApoC3-hypertriglyceridemia (HTG) mice. In the same HTG microenvironment, CD8$^+$ T cell activities were upregulated in ApoC3^{TG} mice but downregulated in P407-treated mice. Increased glycolysis and transcriptome variations in the CD8$^+$ T^{TG} cells indicated that they were stimulated by context cells. The activated macrophages of the ApoC3^{TG} mice stimulated CD8$^+$ T cells and thereby suppressed tumor growth in vivo. Finally, Syk activation induced by ApoC3 in ligation with TLR2/TLR4 stimulated NF-κB/Akt/MAPK signaling and cPLA2. Increased cPLA2 level in macrophages^{TG} not only promoted FFA production and its downstream FAO-associated mROS production but also stimulated TRPM2 and NOX2 for cROS production. Thus, the Syk/cPLA2 signaling axis promoted the alternative and classical modes of inflammasome activation in macrophages^{TG}. A diagram of molecular mechanisms in ApoC3-induced inflammasome activation of macrophage is shown in Supplementary Fig. 9.

PA treatment ex vivo decreased IFN-γ production in CD8$^+$ T cells. However, CD69 and NKG2D expression did not vary remarkably (Fig. 3A). The IFN-γ production of NK cells also decreased after PA treatment [22], indicating that the IFN-γ production of lymphocyte was more sensitively regulated by a high-lipid microenvironment. No obvious variations in CD36 (Fig. 3B) and intracellular FFA (Fig. 3C) levels were found in CD8$^+$ T cells from mice with HTG-plasma. Apoptosis (Fig. 3A) and CD36 (Fig. 3E) expression in the CD8$^+$ T cells were not affected by PA treatment in contrast to those in NK cells [22]. CD8$^+$ T cell activities were relatively stable and inert to be regulated by FFA treatment.

Given upregulated CD8$^+$ T and downregulated NK cell activities [22] were found in the ApoC3^{TG} mice, the retarded tumor growth indicated that overall immune surveillance increased and activated CD8$^+$ T cells predominantly exerted

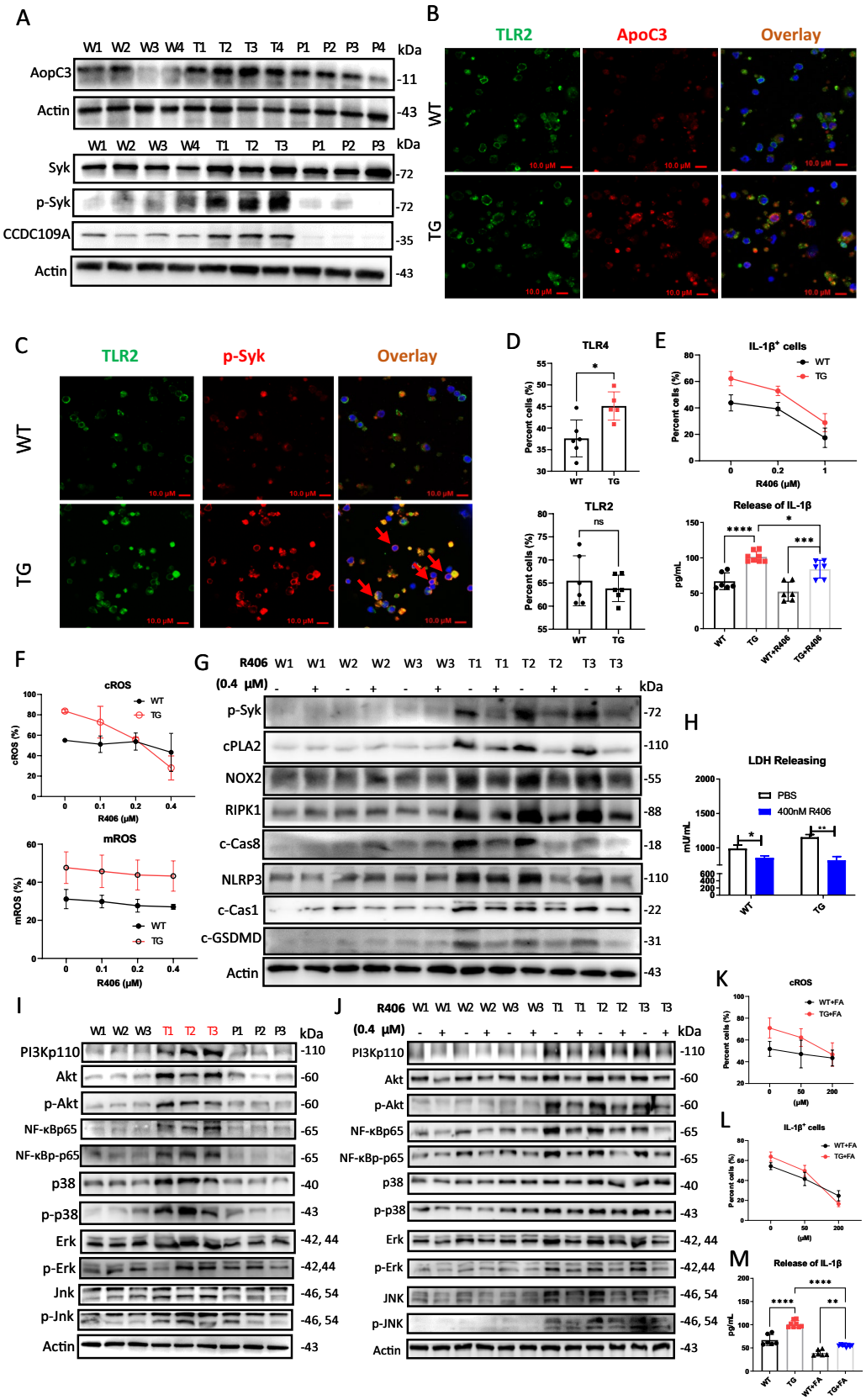
A
W1 W2 W3 W4 T1 T2 T3 T4 P1 P2 P3 P4 kDa
AopC3
-11
Actin
-43
W1 W2 W3 W4 T1 T2 T3 P1 P2 P3 kDa
Syk
-72
p-Syk
-72
CCDC109A
-35
Actin
-43
B
TLR2
ApoC3
Overlay
WT
TG
C
TLR2
p-Syk
Overlay
WT
TG
D
TLR4
Percent cells (%)
WT
TG
TLR2
ns
E
IL-1β+ cells
WT
TG
R406 (μM)
Release of IL-1β
pg/mL
WT
TG
WT+R406
TG+R406
F
cROS
cROS (%)
R406 (μM)
mROS
mROS (%)
G
R406 (0.4 μM)
W1 W1 W2 W2 W3 W3 T1 T1 T2 T2 T3 T3
kDa
p-Syk
-72
cPLA2
-110
NOX2
-55
RIPK1
-88
c-Cas8
-18
NLRP3
-110
c-Cas1
-22
c-GSDMD
-31
Actin
-43
H
LDH Releasing
PBS
400nM R406
mU/mL
WT
TG
I
W1 W2 W3 T1 T2 T3 P1 P2 P3 kDa
PI3Kp110
-110
Akt
-60
p-Akt
-60
NF-κBp65
-65
NF-κBp-p65
-65
p38
-40
p-p38
-43
Erk
-42, 44
p-Erk
-42,44
Jnk
-46, 54
p-Jnk
-46, 54
Actin
-43
J
R406 (0.4 μM)
W1 W1 W2 W2 W3 W3 T1 T1 T2 T2 T3 T3
kDa
PI3Kp110
-110
Akt
-60
p-Akt
-60
NF-κBp65
-65
NF-κBp-p65
-65
p38
-40
p-p38
-43
Erk
-42, 44
p-Erk
-42,44
JNK
-46, 54
p-JNK
-46, 54
Actin
-43
K
cROS
WT+FA
TG+FA
Percent cells (%)
(μM)
L
IL-1β+ cells
WT+FA
TG+FA
Percent cells (%)
(μM)
M
Release of IL-1β
pg/mL
WT
TG
WT+FA
TG+FA

◂**Fig. 7** PLA2 activation in macrophages^{TG} due to the ApoC3-TLR2/4-Syk axis. **A** Protein levels of ApoC3, Syk, p-Syk, and CCDC109A in macrophage lysates were examined. **B**–**C** Co-localization of TLR2 with ApoC3 and p-Syk detected by confocal microscope. **D** Membrane expression of TLR2/TLR4 on macrophages. **E**–**H** Inhibiting Syk (R406) on IL-1β production or secretion, cROS and mROS production, alternative inflammasome activation, and LDH release by macrophages^{TG}. **I**–**J** Detection of activating signaling molecules that generate the signal 1 of NLRP3 inflammasome activation and inhibitory effects mediated by R406 treatment. **K**–**M** Flufenamic acid (FA), an inhibitor of TRPM2, was used in analyzing cROS production and IL-1β production or secretion in macrophages^{TG}. Experiments were repeated twice. *Ns*, no significance. * $P<0.05$, ** $P<0.01$, and *** $P<0.001$

antitumor effects in the ApoC3^{TG} mice. The inhibitory effect exerted by high FFAs and the stimulatory effect exerted by macrophages in the CD8$^+$ T cells were observed in the ApoC3^{TG} mice. Increased CD8$^+$ T cell activity demonstrated that macrophage-mediated activation was more intensive. In the ApoC3^{TG} mice, the effects of lipid-accumulating DCs on CD8$^+$ T cells should not be excluded. However, the DCs of ApoC3^{TG} mice exerted immune-inhibitory activities [22] without Apoc3 expression (Data not shown) and were unable to decrease or increase CD8$^+$ T cell activities (Fig. 5D), suggesting that the activities of CD8$^+$ T^{TG} cells were not affected by DCs. NK cells were easily modulated by HTG-plasma and lipid-accumulating DCs, but CD8$^+$ T cells were preferentially regulated by inflammasome-activated macrophages. This phenomenon indicated inherent differences between NK and CD8$^+$ T cells.

Recombinant ApoC3 induces tenfold less release of IL-1β in murine bone marrow-derived macrophages, as compared with human monocytes [28]. The efficient inflammasome activation of macrophages in ApoC3^{TG} mice was possibly due to the high local levels of ApoC3, which can be produced by macrophages, and efficient and persistent binding of murine ApoC3 with the TLR2/4 of macrophages in mice. Syk activation induced by TLR2/TLR4 cross-linking should be regarded as an initiating signaling event in macrophage activation. As a tyrosine kinase, Syk phosphorylation activated the NF-κB, Akt, and MAPK signaling pathways, which provided the first signal of inflammasome activation. TRPM2 and NOX2 activation by cPLA2 was induced by Syk activation, and FFA generation was promoted by phospholipid hydrolysis. Thus, the elevated cROS production due to NOX2 activation enhanced RIPK1/caspase 8-mediated alternative NLRP3 activation (Signal 2). Although FFAs generated by phospholipid hydrolysis increased FAO and mROS production because signal 2 contributed to classical NLRP3 activation (Fig. 8M–N), mROS-induced inflammasome activation was auxiliary because FAO inhibition by etomoxir did not restore IL-1β secretion to the level as those of macrophages^{WT}. Notably, although macrophages^{TG} increased intake of FFAs and lipoproteins under the HTG microenvironment, they preferentially utilized FFAs from cPLA2-mediated phospholipid hydrolysis in FAO because inhibiting cPLA2 decreased CPT1α level in macrophages^{TG}. All results indicated the key role of Syk activation in the NLRP3 inflammasome activation of macrophages^{TG}.

Decreased ApoC3 expression was observed in liver cancer, and the ApoC3 level was negatively associated with TNM stages in HCC. Meanwhile, high ApoC3 expression in patients with HCC is correlated with increased survival. The positive correlation of ApoC3 expression level with tumor-infiltrated CD8$^+$ T cells in HCC indicated that CD8$^+$ T cell activities regulated by ApoC3 were involved in the progression of HCC. To clarify whether HCC patients with high non-lipoprotein-bound ApoC3 can exert better therapeutic effects with the use of PD-1 antibody is interesting. Given that the genetic polymorphisms of ApoC3 affect its expression level [35], the genotyping of the ApoC3 promoter would help predict the prognosis of patients with HCC. In patients with HCC and high ApoC3 expression, a modified diet with intake of more proteins and less lipids is recommended to decrease FFAs and triglyceride levels in the plasma while high ApoC3 expression is retained.

In summary, high ApoC3 protein alone enhances CD8$^+$ T cell bioactivities in vivo by stimulating the inflammasome activation of macrophages, which is different from effects of ApoC3-induced hyperlipidemia. Increased ApoC3 level in patients with HCC predicted increased survival and was positively associated with CD8$^+$ T cell infiltration. To prevent the side effects of Apoc3-induced hyperlipidemia, the mimetic peptides of ApoC3, which bind with triglyceride to a lesser extent but remain in ligation with TLR2/TLR4, can be a future strategy to target liver cancer.

Supplementary Information The online version contains supplementary material available at https://doi.org/10.1007/s00262-023-03547-8.

Acknowledgements We are grateful to Prof. George Liu and Prof. Qiang You for providing ApoC3^{TG} mice and CD36$^{-/-}$ mice respectively.

Author contributions XJ conceived the study. WG, GL, XH, XJ and ZW designed the experiments. XH, ZL, LL, and SD conducted the experiments. WX, YD, and YZ collected biopsies of HCC. WG, GL,

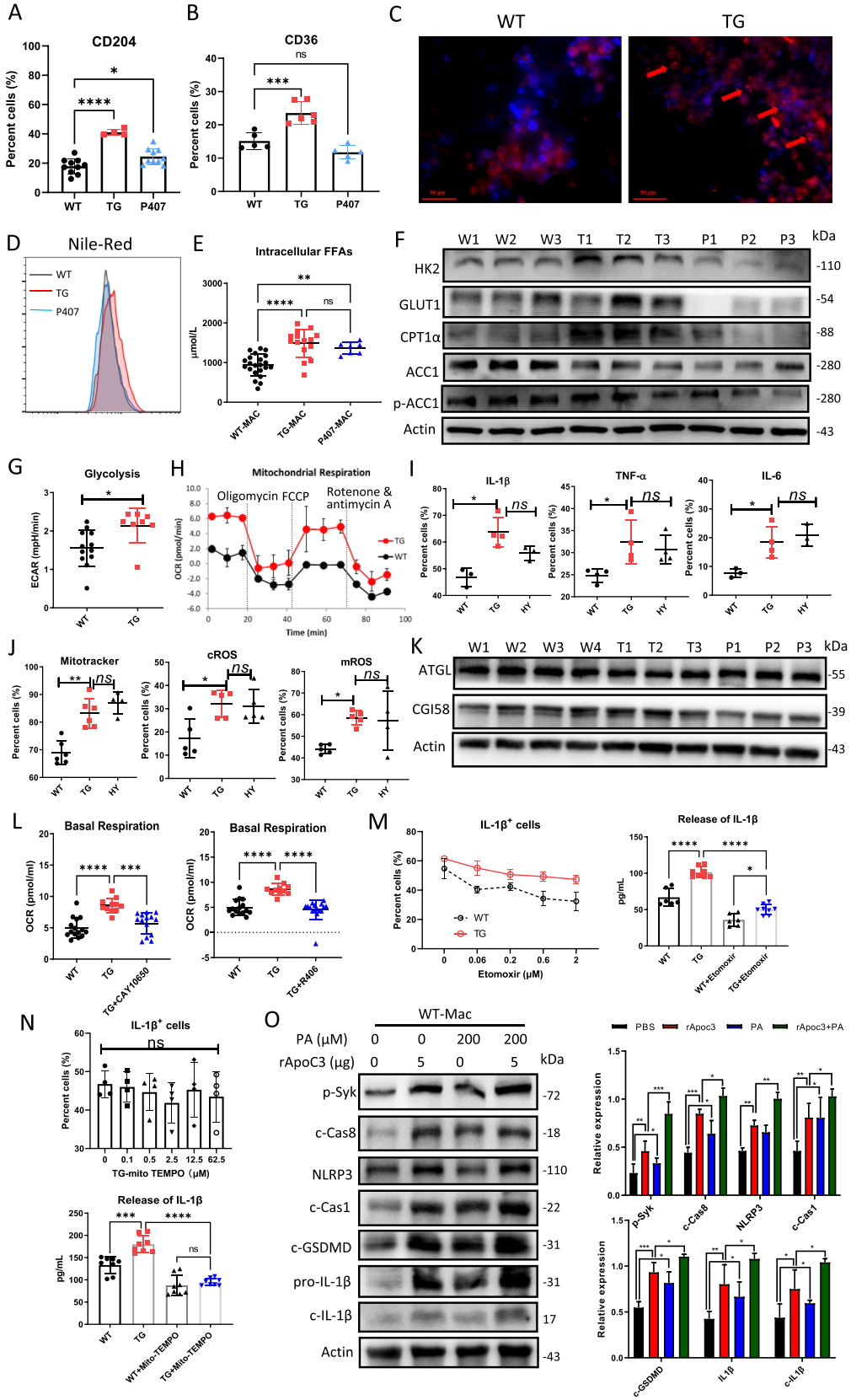
A
CD204
Percent cells (%)
WT
TG
P407
B
CD36
ns
C
WT
TG
D
Nile-Red
WT
TG
P407
E
Intracellular FFAs
μmol/L
WT-MAC
TG-MAC
P407-MAC
F
W1 W2 W3 T1 T2 T3 P1 P2 P3 kDa
HK2
GLUT1
CPT1α
ACC1
p-ACC1
Actin
-110
-54
-88
-280
-280
-43
G
Glycolysis
ECAR (mpH/min)
H
Mitochondrial Respiration
Oligomycin FCCP
Rotenone & antimycin A
OCR (pmol/min)
Time (min)
I
IL-1β
TNF-α
IL-6
HY
J
Mitotracker
cROS
mROS
K
W1 W2 W3 W4 T1 T2 T3 P1 P2 P3 kDa
ATGL
CGI58
Actin
-55
-39
-43
L
Basal Respiration
OCR (pmol/ml)
TG+CAY10650
TG+R406
M
IL-1β+ cells
Etomoxir (μM)
Release of IL-1β
pg/mL
WT+Etomoxir
TG+Etomoxir
N
IL-1β+ cells
TG-mito TEMPO (μM)
Release of IL-1β
WT+Mito-TEMPO
TG+Mito-TEMPO
O
WT-Mac
PA (μM) 0 0 200 200
rApoC3 (μg) 0 5 0 5 kDa
p-Syk
c-Cas8
NLRP3
c-Cas1
c-GSDMD
pro-IL-1β
c-IL-1β
Actin
-72
-18
-110
-22
-31
-31
17
-43
PBS
rApoc3
PA
rApoc3+PA
Relative expression
p-Syk
c-Cas8
NLRP3
c-Cas1
c-GSDMD
IL1β
c-IL1β

◂**Fig. 8** Auxiliary role of mROS in the inflammasome activation of macrophages^{TG}. **A**–**B** CD204 (a scavenger receptor) and CD36 expression in macrophages from WT, TG, or P407-treated mice. **C**–**D** Cellular droplets in macrophages were stained with Nile red and checked by IHC and flow cytometry. **E** Intracellular FFA levels. **F** Levels of enzymes involved in glycolipid metabolism. **G**–**H** Detection of basal glycolysis and OCR. **I** Production of IL-1β, TNF-α and IL-6 in macrophages from WT, ApoC3^{TG} (TG), or ApoC3^{TG}-CD36$^{\pm}$ (HY) mice. **J**–**K** Mitochondria weight, cROS, and mROS, and two lipohydrolases (ATGL and CGI58) in macrophages. **L** Inhibited cPLA2 (CAY10650) or Syk (R406) on basal mitochondrial respiration (OCR). **M** Inhibiting FAO by using a CPT inhibitor (etomoxir) on IL-1β production or secretion in macrophages^{TG}. **N** Depleting mROS by mito-TEMPO on IL-1β production or secretion. **O** Effects of NLRP3 activation in macrophages stimulated by rApoC3, PA, or a combination of rApoC3 and PA. Experiments were repeated twice. *Ns*, no significance. * $P<0.05$, ** $P<0.01$, and *** $P<0.001$

XH and XJ analyzed the data and wrote the manuscript. All authors reviewed the manuscript.

Funding This work was supported by the National Natural Science Foundation of China (Grant Nos. 81873867, 81671547, and 81873866), the Natural Science Foundation of Jiangsu Province, China (Grant Nos. BK20161339, and BK20160479); the "Six peaks" Talent Project of Jiangsu Province.

Data availability The datasets used and/or analyzed during the current study are available from the corresponding author on reasonable request.

Declarations

Conflict of interest There are no financial conflicts of interest with regard to this work.

Ethics approval and consent to participate The study protocol was approved by the ethics committee of the Affiliated Hospital of Yangzhou University and obtained informed consent from all the patients. All animal protocols were approved by the Institutional Animal Care and Use Committee of Yangzhou University.

References

1. Avgerinos KI, Spyrou N, Mantzoros CS, Dalamaga M (2019) Obesity and cancer risk: emerging biological mechanisms and perspectives. Metabol Clin Exp 92:121–135. https://doi.org/10.1016/j.metabol.2018.11.001
2. Bovolini A, Garcia J, Andrade MA, Duarte JA (2021) Metabolic syndrome pathophysiology and predisposing factors. Int J Sports Med 42:199–214. https://doi.org/10.1055/a-1263-0898
3. Kawai T, Autieri MV, Scalia R (2021) Adipose tissue inflammation and metabolic dysfunction in obesity. Am J Physiol Cell Physiol 320:C375–C391. https://doi.org/10.1152/ajpcell.00379.2020
4. Kolb R, Sutterwala FS, Zhang W (2016) Obesity and cancer: inflammation bridges the two. Curr Opin Pharmacol 29:77–89. https://doi.org/10.1016/j.coph.2016.07.005
5. Neganova M, Liu J, Aleksandrova Y, Klochkov S, Fan R (2021) Therapeutic influence on important targets associated with chronic inflammation and oxidative stress in cancer treatment. Cancers. https://doi.org/10.3390/cancers13236062
6. Zhang S, Gang X, Yang S, Cui M, Sun L, Li Z, Wang G (2021) The alterations in and the role of the Th17/Treg balance in metabolic diseases. Front Immunol 12:678355. https://doi.org/10.3389/fimmu.2021.678355
7. Hayashi T, Fujita K, Nojima S et al (2018) High-fat diet-induced inflammation accelerates prostate cancer growth via IL6 signaling. Clin Cancer Res 24:4309–4318. https://doi.org/10.1158/1078-0432.CCR-18-0106
8. Lennon H, Sperrin M, Badrick E, Renehan AG (2016) The obesity paradox in cancer: a review. Curr Oncol Rep 18:56. https://doi.org/10.1007/s11912-016-0539-4
9. Jabbar KJ, Yin CC, Bueso-Ramos CE, Luthra R, Medeiros LJ, Zuo Z (2018) Higher body mass index is associated with better survival in patients with myelodysplastic syndromes. Leuk Res 71:63–66. https://doi.org/10.1016/j.leukres.2018.07.008
10. Schmitz J, Gouni-Berthold I (2018) APOC-III antisense oligonucleotides: a new option for the treatment of hypertriglyceridemia. Curr Med Chem 25:1567–1576. https://doi.org/10.2174/0929867324666170609081612
11. Taskinen MR, Packard CJ, Boren J (2019) Emerging evidence that ApoC-III inhibitors provide novel options to reduce the residual CVD. Curr Atheroscler Rep 21:27. https://doi.org/10.1007/s11883-019-0791-9
12. Khetarpal SA, Zeng X, Millar JS et al (2017) A human APOC3 missense variant and monoclonal antibody accelerate apoC-III clearance and lower triglyceride-rich lipoprotein levels. Nat Med 23:1086–1094. https://doi.org/10.1038/nm.4390
13. Qu S, Perdomo G, Su D, D'Souza FM, Shachter NS, Dong HH (2007) Effects of apoA-V on HDL and VLDL metabolism in APOC3 transgenic mice. J Lipid Res 48:1476–1487. https://doi.org/10.1194/jlr.M600498-JLR200
14. Zha Y, Lu Y, Zhang T, Yan K, Zhuang W, Liang J, Cheng Y, Wang Y (2021) CRISPR/Cas9-mediated knockout of APOC3 stabilizes plasma lipids and inhibits atherosclerosis in rabbits. Lipids Health Dis 20:180. https://doi.org/10.1186/s12944-021-01605-7
15. Alborn WE, Prince MJ, Konrad RJ (2007) Relationship of apolipoprotein A5 and apolipoprotein C3 levels to serum triglycerides in patients with type 2 diabetes. Clin Chim Acta Int J Clin Chem 378:154–158. https://doi.org/10.1016/j.cca.2006.11.009
16. Zhang Y, He W, He C et al (2019) Large triglyceride-rich lipoproteins in hypertriglyceridemia are associated with the severity of acute pancreatitis in experimental mice. Cell Death Dis 10:728. https://doi.org/10.1038/s41419-019-1969-3
17. Tong M, Wang F (2020) APOC3rs2854116, PNPLA3rs738409, and TM6SF2rs58542926 polymorphisms might influence predisposition of NAFLD: a meta-analysis. IUBMB Life 72:1757–1764. https://doi.org/10.1002/iub.2302
18. Pollex RL, Ban MR, Young TK et al (2007) Association between the -455T>C promoter polymorphism of the APOC3 gene and the metabolic syndrome in a multi-ethnic sample. BMC Med Genet 8:80. https://doi.org/10.1186/1471-2350-8-80
19. Miller M, Rhyne J, Chen H, Beach V, Ericson R, Luthra K, Dwivedi M, Misra A (2007) APOC3 promoter polymorphisms C-482T and T-455C are associated with the metabolic syndrome.

Arch Med Res 38:444–451. https://doi.org/10.1016/j.arcmed.2006.10.013
20. Chen W, Zhang F, Xu H, Hou X, Tang D, Dai Y (2022) Identification and characterization of genes related to the prognosis of hepatocellular carcinoma based on single-cell sequencing. Pathol Oncol Res POR 28:1610199. https://doi.org/10.3389/pore.2022.1610199
21. Li X, Wang L, Wang L, Feng Z, Peng C (2021) Single-cell sequencing of hepatocellular carcinoma reveals cell interactions and cell heterogeneity in the microenvironment. Int J Gen Med 14:10141–10153. https://doi.org/10.2147/IJGM.S338090
22. Hu X, Jia X, Xu C, Wei Y, Wang Z, Liu G, You Q, Lu G, Gong W (2021) Downregulation of NK cell activities in Apolipoprotein C-III-induced hyperlipidemia resulting from lipid-induced metabolic reprogramming and crosstalk with lipid-laden dendritic cells. Metab Clin Exp 120:154800. https://doi.org/10.1016/j.metabol.2021.154800
23. Zhou S, Tu J, Ding S et al (2020) High expression of angiopoietin-like protein 4 in advanced colorectal cancer and its association with regulatory T cells and M2 macrophages. Pathol Oncol Res POR 26:1269–1278. https://doi.org/10.1007/s12253-019-00695-0
24. Liu YZ, Cheng X, Zhang T et al (2016) Effect of hypertriglyceridemia on beta cell mass and function in ApoC3 transgenic mice. J Biol Chem 291:14695–14705. https://doi.org/10.1074/jbc.M115.707885
25. Pan Y, Li Y, Gao L et al (2017) Development of a novel model of hypertriglyceridemic acute pancreatitis in mice. Sci Rep 7:40799. https://doi.org/10.1038/srep40799
26. Mossmann D, Park S, Hall MN (2018) mTOR signalling and cellular metabolism are mutual determinants in cancer. Nat Rev Cancer 18:744–757. https://doi.org/10.1038/s41568-018-0074-8
27. Xing YQ, Li A, Yang Y, Li XX, Zhang LN, Guo HC (2018) The regulation of FOXO1 and its role in disease progression. Life Sci 193:124–131. https://doi.org/10.1016/j.lfs.2017.11.030
28. Zewinger S, Reiser J, Jankowski V et al (2020) Apolipoprotein C3 induces inflammation and organ damage by alternative inflammasome activation. Nat Immunol 21:30–41. https://doi.org/10.1038/s41590-019-0548-1
29. Vazquez-Medina JP, Dodia C, Weng L, Mesaros C, Blair IA, Feinstein SI, Chatterjee S, Fisher AB (2016) The phospholipase A2 activity of peroxiredoxin 6 modulates NADPH oxidase 2 activation via lysophosphatidic acid receptor signaling in the pulmonary endothelium and alveolar macrophages. FASEB J Off Publ Fed Am Soc Exp Biol 30:2885–2898. https://doi.org/10.1096/fj.201500146R
30. Lin YC, Huang DY, Chu CL, Lin YL, Lin WW (2013) The tyrosine kinase Syk differentially regulates Toll-like receptor signaling downstream of the adaptor molecules TRAF6 and TRAF3. Sci Signal 6:ra71. https://doi.org/10.1126/scisignal.2003973
31. Means TK, Golenbock DT, Fenton MJ (2000) Structure and function of Toll-like receptor proteins. Life Sci 68:241–258. https://doi.org/10.1016/s0024-3205(00)00939-5
32. Jin MS, Kim SE, Heo JY, Lee ME, Kim HM, Paik SG, Lee H, Lee JO (2007) Crystal structure of the TLR1-TLR2 heterodimer induced by binding of a tri-acylated lipopeptide. Cell 130:1071–1082. https://doi.org/10.1016/j.cell.2007.09.008
33. Kim HM, Park BS, Kim JI et al (2007) Crystal structure of the TLR4-MD-2 complex with bound endotoxin antagonist Eritoran. Cell 130:906–917. https://doi.org/10.1016/j.cell.2007.08.002
34. Sharma BR, Kanneganti TD (2021) NLRP3 inflammasome in cancer and metabolic diseases. Nat Immunol 22:550–559. https://doi.org/10.1038/s41590-021-00886-5
35. Song Y, Zhu L, Richa M, Li P, Yang Y, Li S (2015) Associations of the APOC3 rs5128 polymorphism with plasma APOC3 and lipid levels: a meta-analysis. Lipids Health Dis 14:32. https://doi.org/10.1186/s12944-015-0027-0